Biocompatible wearable touch panel based on ionically conductive organic hydrogels with anti-freezing, anti-dehydration, self-healing, and underwater adhesion properties

Zhenglin Chen[a, b], Jiaqi Yang[c], Likun Zhang[a, b], Haifei Guan[a, b], Zhengyang Lei[a, b], Xiaopeng Zhang[a], Canhui Yang[d], Ying Zhu[a, b], Qianhui Sun[a, b], Lulu Xu[a, b], Ziheng Zhang[a, b], Sen Zeng[a, b], Chuhui Wang[a, b], Rongxu Yan[a, b], Chong Zhang[e, f], Peter E Lobie[a, b, g], Dongmei Yu[h, *], Peiwu Qin[a, b, *], and Can Yang Zhang[a, b, e, *]

[a]Center of Precision Medicine and Healthcare, Tsinghua-Berkeley Shenzhen Institute, Shenzhen, Guangdong Province, 518055, China

[b]Institute of Biopharmaceutics and Health Engineering, Tsinghua Shenzhen International Graduate School, Shenzhen, Guangdong Province, 518055, China

[c]State Key Laboratory of Urban Water Resources and Environment, School of Civil & Environmental Engineering, Harbin Institute of Technology (Shenzhen), Shenzhen, Guangdong 518055, China

[d]Soft Mechanics Lab, Department of Mechanics and Aerospace Engineering, Southern University of Science and Technology, Shenzhen, Guangdong 518055, China

[e]MOE Key Laboratory for Industrial Biocatalysis, Institute of Biochemical Engineering, Department of Chemical Engineering, Tsinghua University, Beijing 100084, China

[f]Center for Synthetic and Systems Biology, Tsinghua University, Beijing 100084, China

[g]Shenzhen Bay Laboratory, Shenzhen, Guangdong 518055, China.

[h]School of Mechanical, Electrical & Information Engineering, Shandong University, Weihai, Shandong 264209, China

Z. Chen, J. Yang, and L. Zhang contributed equally to this work.

* Corresponding authors E-mail address: yudongmei@sdu.edu.cn (D. Yu), pwqin@sz.tsinghua.edu.cn (P. Qin), zhang.cy@sz.tsinghua.edu.cn (C.Y. Zhang).

Abstract: Next-generation touch panels are poised to benefit from the use of stretchable and transparent soft ionic conductors, but these materials face several challenges in practical application, including structural damage, loss of functionality, and device stratification, particularly in extreme environments. To address these challenges, in this work, a biocompatible, transparent, self-adhesive gelatin-PAA-based organic hydrogel (PC-OH) was developed, the gel can adhere to the skin in both air and underwater conditions and also anti-freezing, anti-drying, fast self-healable (with a self-healing time of less than 4s in air and underwater), long-term stable for up to 7 days at a wide range of temperatures, highly stretchable, and conductive over a wide temperature range. Using this organic hydrogel, an organic hydrogel-based surface capacitive touch system has been developed that can detect finger touch position in wet environments and over a wide temperature range, demonstrating its ability to sense finger touch position. The wearable touch panel has been successfully demonstrated through the ability to write text, draw figures, and play electronic games, showcasing its potential use in various applications. This breakthrough has significant implications for the development of next-generation touch panels, particularly in the healthcare, sports, and entertainment industries, where reliable and versatile human-machine interfaces are essential.

Keywords: hydrogels, touch panel anti-freezing, anti-dehydration, self-healing, self-adhesive

1. Introduction

The integrated touch panel plays a critical role in the interaction between the human-machine interface and the display due to its simplicity, portability, and intuitiveness. There are several touch panel technologies available, including capacitive[1–5], resistive[6], optical[7,8], surface acoustic wave[9,10], bending wave[11], piezoelectric[12], and triboelectric (TENG) mechanisms[13,14]. Among them, capacitive touch sensing is widely used in electronic devices such as smartphones, portable computers, gaming consoles, and ticket machines. However, next-generation touch panels require properties such as biocompatibility, stretchability, softness, environmental stability, self-healing, and self-adhesion, which cannot be achieved with conventional touch panels that use indium tin oxide (ITO) as a transparent conductive layer. ITO-based touch panels face significant challenges due to their stiff and brittle properties, which limit their application in next-generation touch panels [15,16] . To address these challenges, researchers have investigated alternative materials such as metal composites [17] , carbon nanomaterials [18] , conducting polymers[5,19], and metal nanowires[20]. However, these materials face challenges such as dramatic sheet resistance increase when stretched, and only a few can be repeatedly stretched, such as conducting polymers and carbon nanotubes (CNTs) [21,22] [21]. Furthermore, biocompatibility needs to be extensively studied for these alternative materials[14,24–28]. On the other hand, conductive hydrogels have attracted considerable attention due to their versatility, transparency, scalability, biocompatibility, and electrical conductivity, making them a valid candidate for next-generation touch panels. Conductive hydrogels have been widely demonstrated in many fields, including microchannels[29], tactile/strain sensors[30,31], diodes/transistors[32,33], human-machine interfaces (e.g., flexible keyboards [34] and touch panels [1–4]), alternating-current electroluminescent devices (ACEL) [35,36] , the actuator [37–40] , energy harvesting/storage devices[39,41] and soft robotics[42].

Hydrogel electronics are susceptible to temperature-induced changes in conductivity and sensing [5,43,44] . The hydrogel inevitably loses its stretchability, conductivity, self-healing, and self-adhesion properties at sub-zero temperatures[43–50].

For ion hydrogels based on ion transport through free water in a polymer network, freezing in the cold reduces the number of free water molecules, thereby slowing the migration of ions[50,51]. Therefore, functional deterioration and signal inaccuracy may result in this case, hindering its practical application at low temperatures. During long-term use, hydrogels' mechanical properties may also be affected by dehydration. In addition, under certain conditions (wet, cold, dry, continuous deformation), adhesion to the substrate can be quickly released, leading to potential delamination of the device and further reducing the reliability of the acquired data. Therefore, it can only be used in additional adhesives like bandages, 3M adhesives, or scotch tapes, while wearable electronics that use these adhesives may have limited biocompatibility when used on the human body[3,4]. Therefore, we are highly interested in developing a hydrogel-based touch panel that is biocompatible, self-healing, environmentally compatible (at subzero and high temperatures), and strongly adhesive (in air and underwater). Many plants and animals in nature (such as tree frogs, red flat bark beetles, *etc*.) can survive in extremely cold weather by preventing ice crystals from forming in their cells[43]. The organisms accumulate cryoprotectants in their tissues, such as urea and glucose, thereby lowering the freezing point of their body fluids[52]. Some cryoprotectants, inorganic salts (e.g., zinc chloride and calcium chloride)[53], organic solvents (*e.g.*, ethylene glycol (EG), glycerol, dimethylsulfoxide (DMSO))[48,50,54], protein[31,51] and ionic liquids (ILs)[55] have been used as an additive for the synthesis of anti-freezing hydrogels inspired by this principle. Organic solvent glycerin is a polyol with a high boiling point, low volatility, and good water solubility. It has the advantages of anti-freezing, low toxicity, and high plasticity. Polyol molecules form molecular clusters with water molecules in the hydrogel matrix, and this can break the hydrogen bond networks of water molecules, hindering interactions between the water molecules themselves, preventing the ice crystals formation (*e.g.*, freezing at low temperatures) and the evaporation of water (*e.g.*, dehydration at high temperatures or for long periods). The presence of glycerol leads to a decrease in the saturated vapor pressure of the binary solution, which results in a decrease in the freezing point of the organic hydrogel and an increase in the resistance to

dehydration [47] . Inspired by natural systems such as mussel and gooseberry, the combinatorial strategy of catechol chemistry and electrostatic kinetics has been used for synthesizing underwater adhesives, and catechol-containing hydrogels have been extensively studied [56,57] . However, these hydrogels usually show weak underwater adhesion when the catechol group acts alone. The strong electrostatic complexation in the gel and abundant catechol groups on the TA surface can jointly promote their durable underwater adhesion [49,58]. Although some progress has been made, there are still problems such as weak underwater adhesion and complicated preparation process, which hinder its further application in wearable flexible electronics. Therefore, it is necessary to develop a new method of preparing hydrogels with high adhesion by simple methods of multiple dynamic interactions inspired by mussels and gooseberries.

In this study, we aimed to improve the anti-freezing and anti-drying abilities of hydrogels by introducing glycerol, as well as to enhance their self-adhesive properties in air and water by incorporating TA and AA-NHS esters with multiple dynamic interactions. The resulting gelatin-PAA-based organic hydrogel (PC-OH) demonstrated remarkable properties, including biocompatibility, high transparency (87 % transmittance of visible light), self-adhesion to the skin both in the air (approximately 967 J/m^2) and water (approximately 428 J/m^2), anti-freezing capabilities (down to -60 ℃), anti-drying capabilities (up to 60 ℃), rapid self-healing (less than 4 seconds in both air and water), long-term stability (up to 7 days) at a wide temperature range (-20 ~ 60 ℃), high stretchability (up to ~1700 % at 60 °C and ~1200 % at -20 °C), and conductivity across a wide temperature range (ionic conductivity of 1.93 S m^{-1} at 60 °C and 3.13 × 10^{-3} S m^{-1} at -30 °C). Moreover, we constructed a surface capacitive touch system based on organic hydrogel to demonstrate its practical application. The results showed that this highly stretchable, transparent, anti-freezing, anti-dehydration, self-healable, and self-adhesive human-machine interface is feasible and can be integrated with the skin under abnormal temperatures and humidity. The touch panel's functionality was demonstrated by writing text, drawing figures, and playing electronic games, indicating its potential

use in various fields requiring reliable electromechanical performance.

2. Results

2.1. Synthesis and characterization of PC-OH

The preparation of biocompatible, transparent, stretchable, anti-freezing and anti-drying, long-term stable, highly conductive, self-healable, and self-adhesive in air and underwater, gelatin-PAA-based organic hydrogel (PC-OH) consists of three main steps, as shown in Fig. 1a. The precursor solution was prepared by firstly dissolving acrylic acid (AA), gelatin, tannic acid (TA), acrylic acid n-hydroxysuccinimide ester (AA-NHS), aluminum chloride ($AlCl_3$), photo-crosslinker gelatin methacryloyl (GelMA) and UV initiator α-ketoglutaric acid (AKG) in Milli-Q water, and then the gelatin-PAA based hydrogel (PC-H) was obtained by UV curing the precursor solution. Finally, Gelatin-PAA based organic hydrogel (PC-OH) was prepared by immersing the obtained gelatin-PAA-based hydrogel (PC-H) in water/glycerol binary solvent (1:1 (v/v)) for 4 hours. During the soaking process, water molecules in the PC-H hydrogel are partially replaced by glycerol molecules. At the same time, a large number of hydrogen bonds form between the gelatin and glycerol, causing the hydrogel to transform into an organic hydrogel. This transformation endows the organic hydrogel with excellent anti-freezing and anti-drying properties.

Various compounds are involved in PC-OH organic hydrogel network to perform specific functions (Fig. 1b). In the network, gelatin, and PAA can form a double network structure. The physically cross-linked gelatin network will act as a sacrificial bond during deformation to improve the recovery ability of the hydrogel and realize dynamic energy dissipation of the organic hydrogel. The chemically cross-linked PAA network improves the mechanical strength of the organic hydrogel. In the network, various interactions are included to enhance the adhesion of hydrogels in water and air (*e.g.*, hydrogen bonds, covalent bonds, and electrostatic interactions). The organic hydrogel surface is highly adhesive in air and water by using tannic acid (TA) containing large amounts of catechol and pyrogallol groups and AA-NHS esters with positively charged primary amine groups. TA is a biocompatible polyphenolic compound widely used as a self-adhesive monomer with excellent adhesion properties

as its high content of catechol and pyrogallol groups (25 hydroxyl and 10 carbonyl groups). Thereby TA can form hydrogen bonds with Gelatin-PAA chains. The free catechol/pyrogallol groups in TA enable the organo-hydrogel to form hydrogen bonds, ionic coordination, and Michael addition at the matrix interface, improving the interfacial bonding at the organic hydrogel-tissue interface. The AA-NHS ester group can form covalent amide bonds with the skin, promoting fast and strong adhesion at the organic hydrogel-tissue interface through amide covalent cross-linking. To optimize the performance of the organic hydrogels, $AlCl_3$ was added to the organic hydrogels to obtain excellent electrical conductivity and sensing properties by freely moving aluminum (Al^{3+}) and chloride (Cl^-) ions and to form metal ion coordination interactions with free carboxyl groups on PAA chains and phenolic hydroxyl groups on TA in the cross-linked network, which enhanced the mechanical strength of the organic hydrogels and met the requirements of ion electronics devices[59].

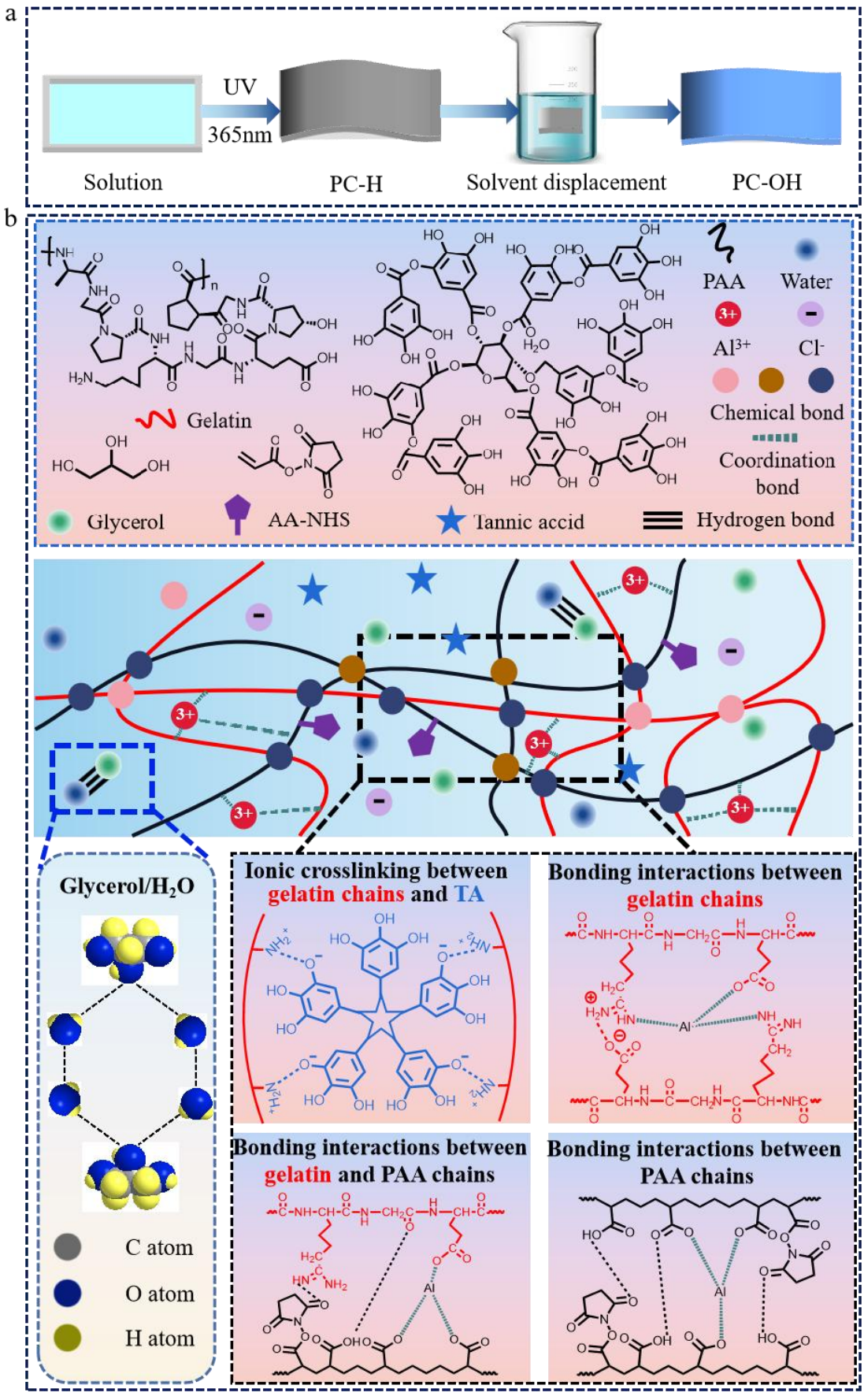

Fig. 1. Schematic diagram of the preparation of PC-OH organic hydrogels. Scheme of

the synthesis process of PC-OH (a). The physicochemical network structure and mechanism of PC-OH (b).

To maintain the mechanical properties of the organic hydrogel in various environments, we introduced a glycerol-water binary solvent system as it can effectively lower the network's freezing point, thus hindering water's evaporation and the formation of ice crystals below zero degrees (Fig. 1b). Meanwhile, due to the formation of a large number of hydrogen bonds between water and glycerol, the PC-OH organic hydrogel has good water retention properties. Therefore, PC-OH organic hydrogels synthesized in this work can be used in practical applications for a long time.

To evaluate the morphology of the organic hydrogels, the PC-H and PC-OH samples were characterized by scanning electron microscopy (SEM) (Fig. 2a and b). As shown in Fig. 2a, the PC-H hydrogel surface appears relatively sparse, with pores of varying sizes. This unique porous structure provides a pathway for the movement of conducting ions, thereby giving it high electrical conductivity. On the other hand, as seen in Fig. 2b, PAA-OH has a smooth and flat morphology due to the increased cross-link density resulting from the presence of glycerol.

The interaction network of the PC-OH organic hydrogel was confirmed using Fourier-transform infrared spectroscopy (FTIR) (Fig. 2c). Significant absorption bands were observed at approximately 1635 and 1230 cm^{-1} for the carboxyl group C=O stretching vibration and the NHS ester C-N-C stretching vibration, respectively. This indicates successful grafting of the NHS ester on the gel network polymer chain. Additionally, characteristic peaks corresponding to O-H stretching vibrations appeared for both PC-H and PC-OH at approximately 3340 cm^{-1}. In the presence of glycerol, the PAA-OH absorption band was more pronounced than that of PC-H, indicating that the stretching vibration of OH was enhanced.

Furthermore, the ability to see the skin's condition is an essential feature of wearable sensor devices. Ionic conductive hydrogels are effective methods for preparing transparent and highly resilient hydrogels. PC-H hydrogels and PC-OH

organic hydrogels are transparent by ultraviolet-visible-near infrared spectrophotometry (UV-Vis-NIR) analysis in the visible band of 400 ~ 800 nm. In contrast, the PC-OH organic hydrogels are more transparent, with the light transmission of PC-OH exceeding 87% (Fig. 2d and e). The ideal transparency of PC-OH organic hydrogel shows great promise for its application in the field of wearable sensors for visual interaction. The ideal wearable touch panel should be non-toxic and biocompatible.

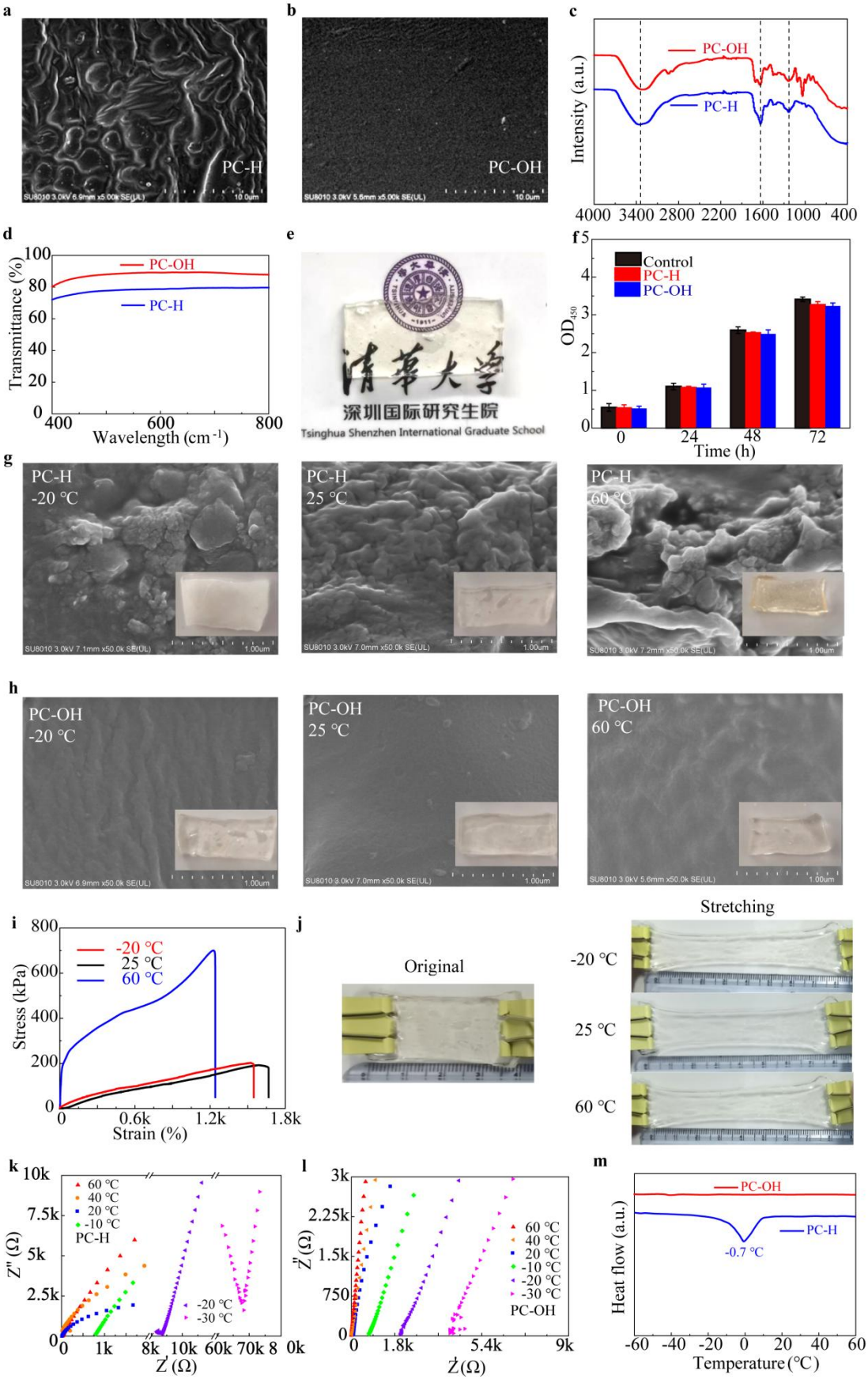

Fig. 2. Physical properties and biocompatibility of PC-OH organic hydrogels. SEM

pictures of PC-H (a) and PC-OH (b). ATR-FTIR of PC-H and PC-OH (c). Transmission spectra of 2.0-mm thick PC-H and PC-OH films (d). Photographs of logo and text covered by 2.0-mm thick PC-OH films (e). Cell proliferation was assessed by the CCK-8 assay of PC-H and PC-OH after 24h, 48h, and 72h of A549 cells incubation, Control: Deionized dwater (Milli-Q, 18.2 MΩ cm^{-1}) (f). SEM images of PC-H at -20, 25, and 60 ℃ (g) and PC-OH at -20, 25, and 60 ℃ (h). Inset: digital photos of PC-H and PC-OH at -20, 25, and 60 ℃. Stress-strain curves of PC-OH at different temperatures (-20, 25, and 60 ℃ (i). Digital photos of original PC-OH and tensile performance at -20, 25, and 60 ℃ (j). Demonstration of the electrical property of PC-OH: Nyquist plots of PC-H (k) and PC-OH (l) at determined temperatures from -20 ~ 60 ℃. DSC curves of PC-H and PC-OH (m).

To investigate PC-OH biocompatibility quantitatively, we used fluorescence imaging and the MTT assay to evaluate PC-OH extracts'OH extracts' in vitro cell viability [27] (Supplementary Fig. 1). Live cells were observed by confocal laser scanning microscopy (CLSM). CLSM images showed no significant decrease in cell viability in the PC-OH extract hydrogel medium culture compared to the control group. Growth curves of A549 cells [26] (Fig. 2f) showed proliferation levels of these cells with different treatments of PC-H and PC-OH at different time points (24h, 48h, and 72h), CCK-8 assay was used to determine the cell viability, as shown in Fig. 2f, the viability of A549 cells treated with PC-OH no significant difference from that of the control group (after 72h incubation, the absorbance of the control and PC-OH treated A549 cells at 540 nm were 3.41 and 3.24, the difference is less than 5%). These results indicate that PC-OH has good biocompatibility and can be used for biocompatible wearable electronic device applications.

2.2. Anti-freezing and anti-dehydration properties of PC-OH

For hydrogel-based electronics, the temperature is one of the most crucial limitations for its practical applications, the electronics will freeze at sub-zero temperatures and dehydrates at high temperatures, and as a result, various excellent properties will be lost. Compared to other bio-inspired neutral substances (*e.g.*, ethylene glycol (EG) and dimethyl sulfoxide (DMSO))[46] and pure concentrated salts

(*e.g.*, lithium chloride (LiCl), sodium chloride (NaCl), and calcium chloride ($CaCl_2$)) [60] , especially at high concentrations, glycerol was chosen as a hygroscopic/anti-freezing material due to its low biotoxicity in skin-worn sensing processes, as well as due to its neutrally charged nature, it also causes minor damage to the ionic crosslinking network and charging groups within the adhesive layer, and glycerol makes organic hydrogels effective anti-freezing and anti-dehydration properties by breaking the hydrogen bonds between water molecules and forming strong hydrogen bonds with water molecules[46,54]. The development of glycerol-based organic hydrogels eliminates the adaptability of stretchable wearable electronics at different temperatures, which ensures excellent mechanical and electrical conductivity.

SEM characterization was conducted to investigate the ability of PC-OH to withstand extreme temperatures. Fig. 2g and h shows that the microstructure of PC-H is damaged under -20 ℃ and 60 ℃, whereas there is no significant difference in PC-OH, indicating that the PC-OH microstructure remains intact at extreme temperatures. This is due to the high number of hydrogen bonds between water and glycerol in the organic hydrogel network, which limits the formation of ice crystals and evaporation of water, allowing PC-OH to maintain its microstructure under abnormal temperatures. Optical photographs of PC-H and PC-OH were taken after storage for 24 h at -20°C, 25°C, and 60°C, as shown in the insert in Fig. 2g and h. At -20°C, the PC-H hydrogel becomes stiff and brittle due to complete freezing, while the PC-OH organic hydrogel remains barely visible to the naked eye and can withstand ≈1500% strain (Fig. 2i and j, and Supplementary Fig. 2 and 3). At 60°C, the PC-H hydrogel loses elasticity and function due to water loss, while the PC-OH organic hydrogel still maintains excellent tensile properties and can withstand ≈1200% strain due to the presence of glycerol solvent. The presence of a large number of hydrogen bonds between water and glycerol molecules hinders water loss and thus maintains the gel's stable mechanical properties. Interestingly, the fracture tensile strength of PC-OH organic hydrogels significantly increased at the high temperature (60 ℃) compared to low temperatures (-20 ℃) and room temperature (25 ℃). This could be explained by increased water loss at higher temperatures, which also facilitates the hydrogen bonds formed between

polymer chains, thereby improving the mechanical properties of PC-OH organic hydrogels, such as Young's modulus and fracture stress[44].

Excellent conductivity is vital in achieving stable sensing of hydrogel-based electronic devices. However, maintaining relatively stable conductivity under various conditions, from low temperatures (-20 ℃) to high temperatures (60 ℃), remains challenging. Fig. 2k and l show the Nyquist plots of PC-OH organic hydrogels and PC-H hydrogels. From the results, we can see that the conductivity of PC-OH organic hydrogel is less affected by temperature than that of PC-H hydrogel. The electrical conductivity (σ) can be calculated from the plots by $\sigma = d/RS$, where d is the thickness of the gels, S is the area of the gels, and R is the point value intersecting the Z' axis where the plot is located. As shown in Supplementary Fig. 4, the conductivity of the PC-OH organic hydrogel decreases with the temperature at 60 ℃ and -30 ℃, with 1.93 S m^{-1} and 3.13 × 10^{-3} S m^{-1}, By contrast, the conductivity of the PC-H hydrogel decreases substantially with decreasing temperature, being 1.38 S m^{-1} at 60 ℃ and 1.87 × 10^{-4} S m^{-1} at -30 ℃, which is strongly related to the freezing and dehydration of hydrogels at low and high temperatures. The water crystallization in the hydrogel network at freezing temperatures can hinder the movement of ions, resulting in an ionic conductivity decrease. The dehydration of the gel at high temperatures will also lead to the evaporation of its water, which decreases the $AlCl_3$ solubility in the solvent, resulting in an ionic conductivity decrease. However, after experiencing different temperatures, it was observed that the conductivity of PC-OH did not change as dramatically as that of PC-H. The environmental adaptability of organic hydrogels can explain this phenomenon. In the hydrogel network, multiple water molecules and glycerol hydrogen bonds improve the anti-freezing and anti-dehydration ability. In addition, the conductivity results at these temperatures show that PC-H cannot withstand an extensive temperature range. The ionic conductivity decreases with decreasing temperature, whereas the conductivity of PC-OH can remain relative stability at different temperatures (-20 ~ 60 ℃) (Fig. 2k). To further demonstrate the anti-freezing of PC-OH organic hydrogels, the anti-freezing of PC-OH organic hydrogels and PC-H hydrogels were evaluated by differential scanning calorimetry

(DSC). From the results, we can see that PC-H showed a crystallization peak at -0.7 °C, which may be because the ice crystals from the "free water" appeared in the PC-H hydrogel. It is worth noting that the DSC curve of PC-OH showed no crystallization peak at -60~60 °C (Fig. 2m), indicating no ice crystal formation in the PC-OH organic hydrogel. Conventional hydrogels are usually frozen at sub-zero temperature conditions due to their high content of aqueous solvents. Soft hydrogels usually turn into solids as hard as ice, which inevitably leads to a decrease in properties (*e.g.*, electrical conductivity, transparency, and elasticity). Strong hydrogen bonds between the glycerol, polymer matrix, and water molecules can be formed due to the addition of glycerol to the hydrogel, which inhibits PC-OH from freezing at subzero temperatures.

2.3. Long-term stability of PC-OH organic hydrogel

Soft materials such as hydrogel remain a major challenge in terms of dehydration after long-term use in their practical application, which may lead to structural and functional failures because of moisture loss, thus hindering long-term use in wearable electronics [46,47,51] . To evaluate the mechanical stability of PC-H and PC-OH, the samples of PC-H and PC-OH (L×W×H: 20.0 × 10.0 × 2.0 mm^3) were first kept at room temperature (25 °C, 38 % RH) for 7 days. Several mechanical loads (e.g., stretch, bend, and twist) were applied to the samples. It can be seen from Fig. 3a that PC-H lost its elasticity and stretchability due to water loss, while PC-OH could be reversibly stretched, bent, and twisted. In addition, tensile tests were operated to study the mechanical properties of PC-OH after 7 days of being kept at room temperature (25 °C, 38 % RH) compared to original conditions (Fig. 3b). The results show that the failure strain of PC-H decreased dramatically (<10%) after 7 days of storage compared to original conditions (≈1600%). In comparison, PC-OH can tolerate more than 600% strain even after 7 days. In addition, Young's modulus of PC-H increased significantly with time from 0.32 to 283.75 MPa. In comparison, PC-OH could remain at a relatively low level (from 0.72 to 3.65 MPa) (Fig. 3c). A sharp water loss from the hydrogel network caused these significant changes in the PC-H mechanical

parameters. On the contrary, the water retention of PC-OH is enhanced by the presence of glycerol, as it can form hydrogen bonds with water molecules to mitigate water evaporation.

The changes in mass and conductivity of PC-H and PC-OH samples were also studied after being kept at room temperature for 7 days to investigate the environmental stability of PC-OH at room temperature after long-term use (Fig. 3d). From Fig. 3d, we can see that the mass of PC-OH increased slightly at the beginning and then decreased with time, dropping to 90% of the initial state on the seventh day, which is because that the presence of a large number of hydroxyl groups in the glycerol chain, resulting in a lower water vapor pressure in the PC-OH gel matrix than in the environment. Conversely, the mass of PC-H hydrogels decreased rapidly and consistently to 20% of the original mass after 7 days of storage at room temperature, and this significant mass reduction was because the original hydrogel matrix without the addition of glycerol had a higher internal vapor pressure of water than in the environment. The conductivity of PC-H hydrogel also showed a decreasing trend (about 0.001 S m^{-1} after storage for 7 days) due to the gradual evaporation of water molecules in the PC-H hydrogel network over time, thus limiting the movement of ions (Fig. 3e). In contrast, PC-OH only experienced a few decreases in conductivity (because water evaporation increased the concentration of polymer chains and decreased the mobility of ions) during 7 days of storage in high humidity conditions (RH=65%). However, the conductivity level of ≈0.1 S m^{-1} was still sufficient for sensing after 7 days of storage. This phenomenon can be explained by the fact that the ionization constant of glycerol is lower than water, making the solvent molecules easier to dissociate and producing more free-flowing ions (i.e., H+). In addition, the addition of glycerol can improve the organic hydrogels' water retention because the abundant hydroxyl groups in the hydrogel can allow the glycerol to form strong hydrogen bonds with water molecules, thereby reducing the loss of water and keeping the ionic conductivity relatively high for 7 days (100 times higher than PC-H after 7 days storage). In addition, $AlCl_3$ plays a key role in improving the ionic conductivity of PC-OH organic hydrogels by dissolving in water, interacting with carboxylate ions

and phenolic hydroxyl groups in the organic hydrogel network by dissolving in the organic hydrogel network, $AlCl_3$ can improve the conductivity of organic hydrogels as it can move freely in the organic hydrogel network by hydrating with water molecules through hydrogen bonds

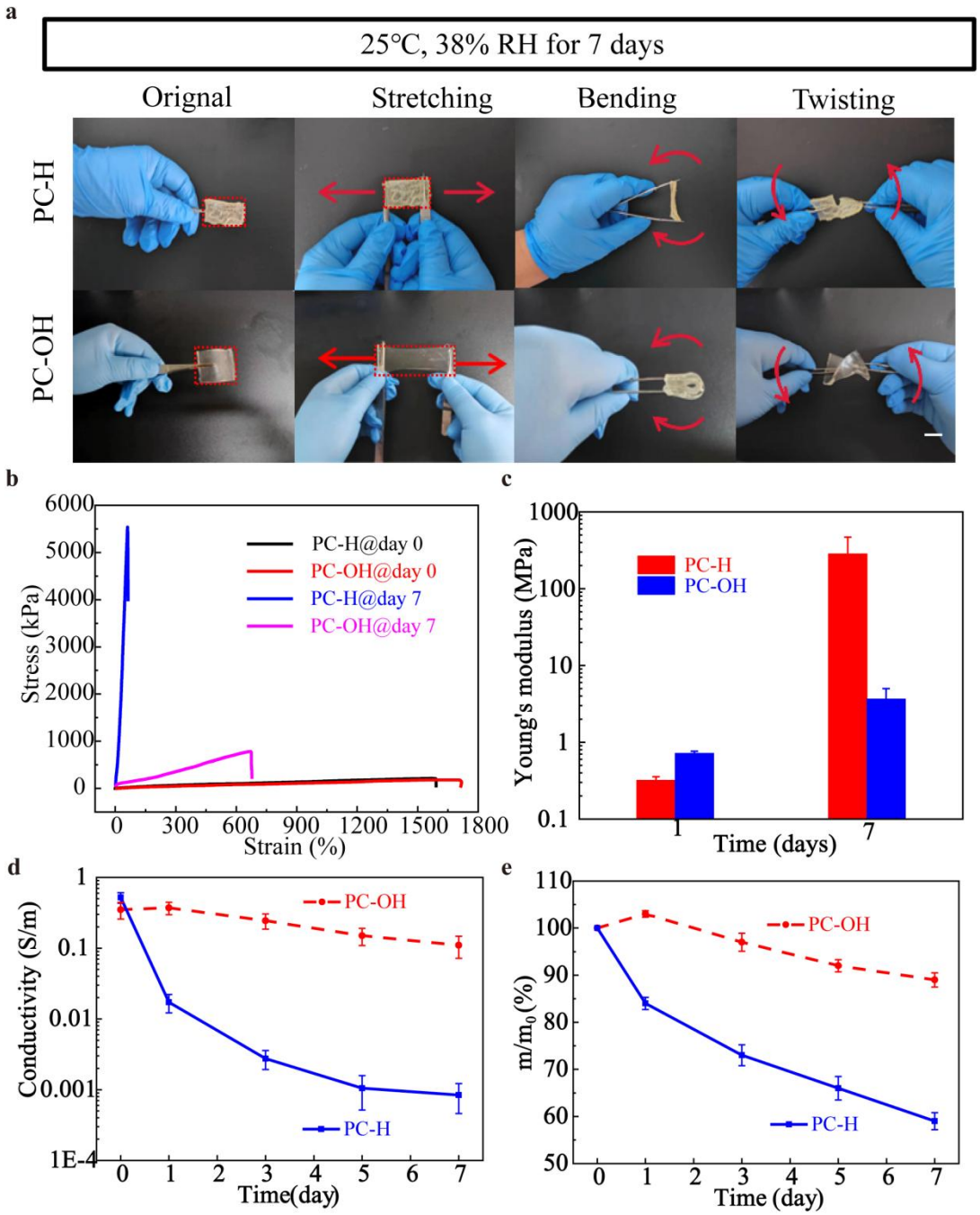

.

Fig. 3. Environmental stability of PC-OH. Photographs of PC-H and PC-OH in tension, bending, and twisting after 7 days of storage at room temperature (a). Photographs of PC-H and PC-OH at room temperature for 7 days (b). Photographs of PC-H and PC-OH at room temperature for 7 days (c). Variation of mass of PC-H and PC-OH at room temperature for 7 d with time (d). Variation of conductivity of PC-H and PC-OH with time at room temperature for 7 days (e).

2.4 Electromechanical self-healing properties of PC-OH

Wearable and stretchable ionic electronics are often under large amounts of repetitive stresses and external forces that can easily lead to material mechanical damage such as abrasion, scratches, and cuts, which can shorten their lifetime. The ionic electronic devices' lifetime can be improved by developing and integrating organic hydrogels with self-healing abilities. The PC-OH organo-hydrogels can be autonomous electromechanical self-healable, further demonstrated in this study by repairing visible cuts on the material. First, the sample was cut into two separate pieces. Then the two sections were gently reconnected before the polymer chains in the hydrogel could diffuse into the interface over time. A topological entanglement could be formed with the other part network, finally allowing the hydrogel to be healed without adding additional materials. Without any stimulation, the two pieces of separated PC-OH exhibited good mechanical self-healing properties upon contact. Fig. 4a is the optical microscope image of the organic hydrogel sample self-healing process when kept at room temperature for 24 h. It can be seen that the cut interface has disappeared after 24 h of self-healing (Supplementary Movie 1). In this work, we defined the recovered strain to the original strain ratio as the mechanical self-healing efficiency.

All cut self-healed PC-OH organic hydrogels maintained a similar Young's modulus and followed tensile stress distribution at different temperatures (-20 ~ 60 °C) underwater. The mechanical properties of PC-OH are self-recovered at all temperatures, even at low temperatures of -20 °C. As shown in Fig. 4b, the mechanical self-healing efficiencies were 87.58 %, 90.8 %, and 92.3 % after self-

healing for 24 h at different temperatures (-20, 25, and 60 °C). It also can be seen from the results that the mechanical self-healing efficiency of PC-OH increased with increasing temperature and self-healing time, showing that the thermal movement of the polymer accelerates and meantime promotes the new cross-link site generation. Impressively, the PC-OH organic hydrogel also has a strong underwater self-healing ability.

As shown in Fig. 4c, after self-healing in water at 25 °C for 24 h, the tensile stress, and strain of the healed PC-OH organic hydrogel were ≈ 0.12 MPa and ≈ 1100%, respectively, relative to the immersed pristine sample, the mechanical self-healing efficiency of PC-OH was more than 88%. Besides the mechanical self-healing ability, the electrical self-healing ability of hydrogels is also crucial to the durability of ionic electronic devices. In this work, the ionic conductivity of PC-OH organic hydrogels is also self-healable. Fig. 4d and e show a photograph of the PC-OH organic hydrogel strip, which is connected with a red light-emitting diode (LED) in series at room temperature. We first cut the strip into two parts, then immediately reconnected the two parts and illuminated the red LED. It can be seen that after gentle stretching, the PC-OH organic hydrogel mechanical self-healing was observed, and the red LED is illuminated even in the stretched state, indicating that the PC-OH organic hydrogel has reliable electromechanical self-healing abilities.

The in situ and real-time electrical self-healing ability of PC-OH organic hydrogel is demonstrated in Fig. 4f. At first, the current in the PC-OH organo-hydrogel strip was stable. Then the PC-OH organo-hydrogel strip was quickly cut into two parts with a sharp ceramic knife. At that point, a downward peak of the current immediately appeared, indicating that the ion transport pathway in the separated part was discontinuous. After the two parts separated completely, the current dropped to 0. Then reconnecting the two separated parts, it can be seen that within only 4 seconds, the current can recover to 87% of the initial current, indicating that the organic hydrogel is electrically self-healable when the ion transport channel is reconstructed. As the reconstruction of ion channels allowed the electrical conductivity of PC-OH to

be restored, the current in the cut-reconnected PC-OH after self-healing at -20°C, 25°C, and 60°C can be gradually recovered within 24 h, corresponding to electrical 89%, 94%, and 98% self-healing efficiencies, respectively. It can also be seen from Fig. 4g that PC-OH has an electrical self-healing efficiency greater than 92% after 24 h of self-healing in water at 25°C. These results indicate the PC-OH has the ability of autonomously electrical self-healing after being damaged at an extensive temperature range of air (-20 ~ 60°C) and underwater.

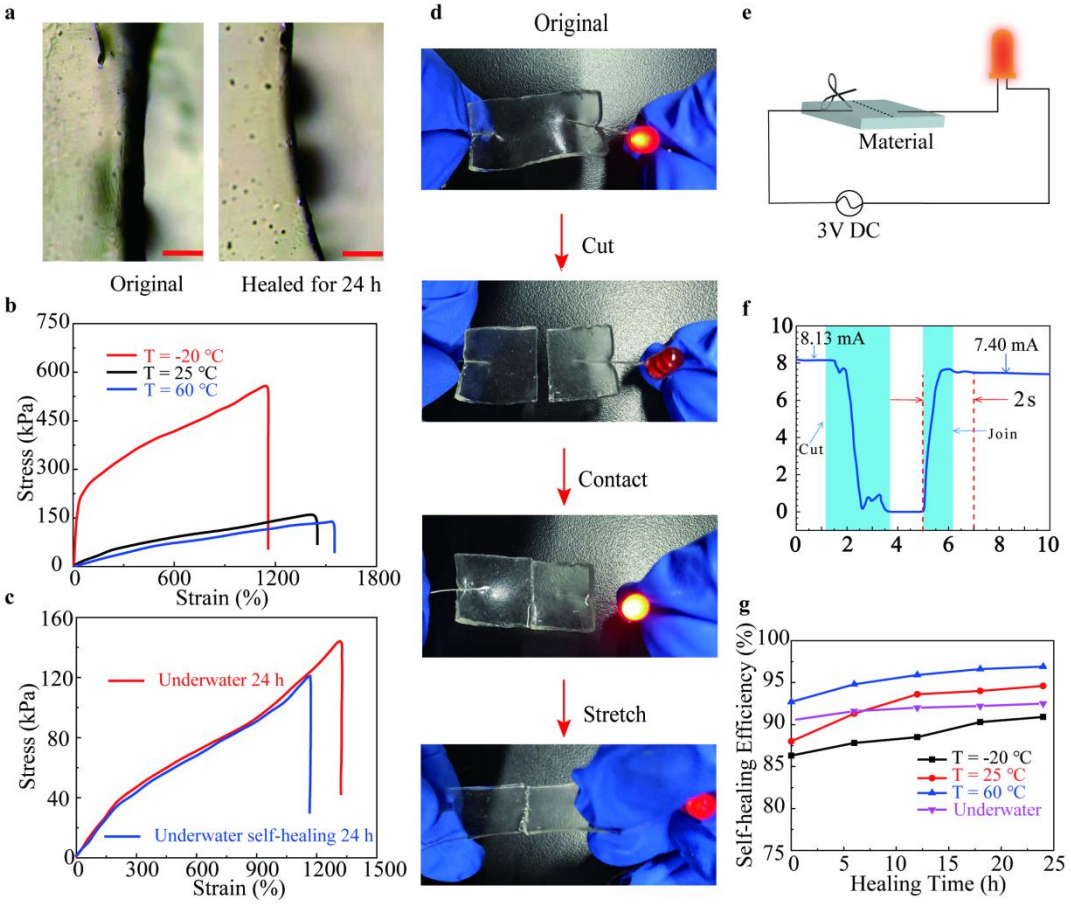

Fig. 4. Electromechanical self-healing performance of PC-OH. Optical microscope images of the PC-OH organic hydrogel autonomous self-healing process at 25 °C (a). After self-healing at -20, 25, and 60 °C with 24 h (b), the stress-strain curves of PC-OH specimens. After 24 h storage and self-healing underwater at 25 °C (c), the stress-strain curves of PC-OH specimens. The self-healing process using red LED demonstrates PC-OH's conductivity (d, e). Current flowing through PC-OH Vs. Time of PC-OH organic hydrogel in its original state, cut and reconnected at 25°C (f).

Electrical self-healing efficiency Vs. Self-healing time after 24 hours of storage in different environments (-20, 25, 60°C and underwater) (g).

2.5 Adhesion property of PC-OH in air and underwater

The adhesive ability of the hydrogels is critical to ensure reliable functionality in hydrogel-based flexible wearable ionic electronics, which can ensure a consistent and stable connection between the electrodes of the electronics and the underlying substrate, thereby reducing the use of external auxiliary tapes with large interfacial resistance and the severe motion artifacts caused by the tapes [45] . In the PC-OH network, multiple interactions play a crucial role in adhesion, including hydrogen bonding and multiple electrostatic interactions between the amino groups in the tissue and the functional groups in the organic hydrogel (e.g., dynamic catechol chemistry of TA, carboxyl groups of PAA, and hydroxyl groups in the solvent system) [56] . In addition, the amide bonding covalent interactions between the active-NHS groups and the amino groups of the tissues at the hydrogel-tissue interface contribute to the tough adhesion of the hydrogel on the human skin. As seen in Fig. 5a, PC-OH organic hydrogels can adhere tightly to the surfaces of various inorganic and organic substrates, including plastic (pe), paper (cellulose), glass, stone, steel, and rubber, making PC-OH organic hydrogels widely used in different substrates. As shown in Fig. 5b, a lap shear test was performed by sandwiching a hydrogel assembly between a pair of substrates to measure the adhesive strength. The maximum adhesion strength was employed as the interfacial adhesion strength at the time of interfacial disruption. From the results, we can see that the adhesive strengths were 11.5, 9.2, and 5.1 kPa for the stone/skin, paper/skin, and glass/skin interfaces, respectively (Fig. 5c). It can be seen that the maximum adhesive strength of the stone and paper substrates is much higher than glass substrate, this is mainly attributed to the rough surface of the stone and paper, this is because that the rough surface can increase the contact area of the substrates with the PC-OH organic hydrogel. From the adhesion results, it is clear that the PC-OH organic hydrogel exhibits good shear test performance, which can be explained by the fact that the adhesion of the PC-OH organic hydrogel dissipates

energy during the peeling process, thereby can help the hydrogel to maintain a more significant peeling force.

PC-OH organic hydrogels can adhere firmly to the metal without the adhesion being weakened by excess water. In contrast, PC-OH can adhere even to metals in water (Fig. 5d). Adhesion on human skin in the air and underwater has also been demonstrated, as shown in Fig. 5e and f. It can be seen that PC-OH can adhere tightly to the forearm of the human, when the end of the PC-OH organic hydrogel was applied with peeling force, the skin conformed to the PC-OH. Then it was pulled up in the air and underwater, showing excellent adhesion properties of PC-OH in the air and underwater. Next, to quantitatively characterize the underwater adhesion properties of PC-OH, the interfacial adhesion between PC-OH and skin under normal and humid conditions were tested by the lap shear test. Notably, we tested the interfacial adhesion of porcine skin to PC-OH organic hydrogel (contact area: 10.0 mm × 10.0 mm) as the porcine skin's similarity to human skin. The interfacial adhesion energy between the PC-OH organic hydrogel and the porcine skin was approximately ≈ 967 $J \cdot m^{-2}$ in the air, making stable adhesion of wearable sensing possible, as shown in Fig. 5g and h. During water immersion, the adhesion energy tends to decrease because water inhibits the interfacial interaction and hinders the conformal contact at the interface between the two objects.

Nevertheless, it is still possible for the hydrogel to maintain high adhesion energy (≈428 J/m^{-2}). It should be noted that the tough adhesion of organic hydrogels on different surfaces (rigid metal electrodes or flexible polymer substrates metal electrodes or flexible polymer substrates) is beneficial for applications in soft electronic systems since many wearable applications inevitably expose devices to liquids (e.g., sweat and rain). The excellent adhesion of PC-OH organic hydrogels may be a synergistic effect of chemical interaction and energy dissipation during the peeling process (Fig. 5i). As the existence of abundant functional groups in the PC-OH organic hydrogels, especially the phenolic hydroxyl group in TA, and also -NHS groups in AA-NHS ester, various noncovalent interactions (e.g., ion−dipole, metal coordination bonds, and hydrogen bonds), will be formed between the PC-OH organic

hydrogels and the substrates[45]. On the other hand, in PC-OH organic hydrogels, the existence of dynamic metal coordination bonds and hydrogen bonds can provide dissipation mechanisms for the interface, resulting in additional energy required for the expansion of interfacial cracks. These results suggest that the strong adhesion of the PC-OH organo-hydrogel developed in this work to different surfaces (rigid metal electrodes or flexible polymer substrates) in air and underwater may facilitate the application of organic hydrogel in soft electronic systems, especially in humid conditions.

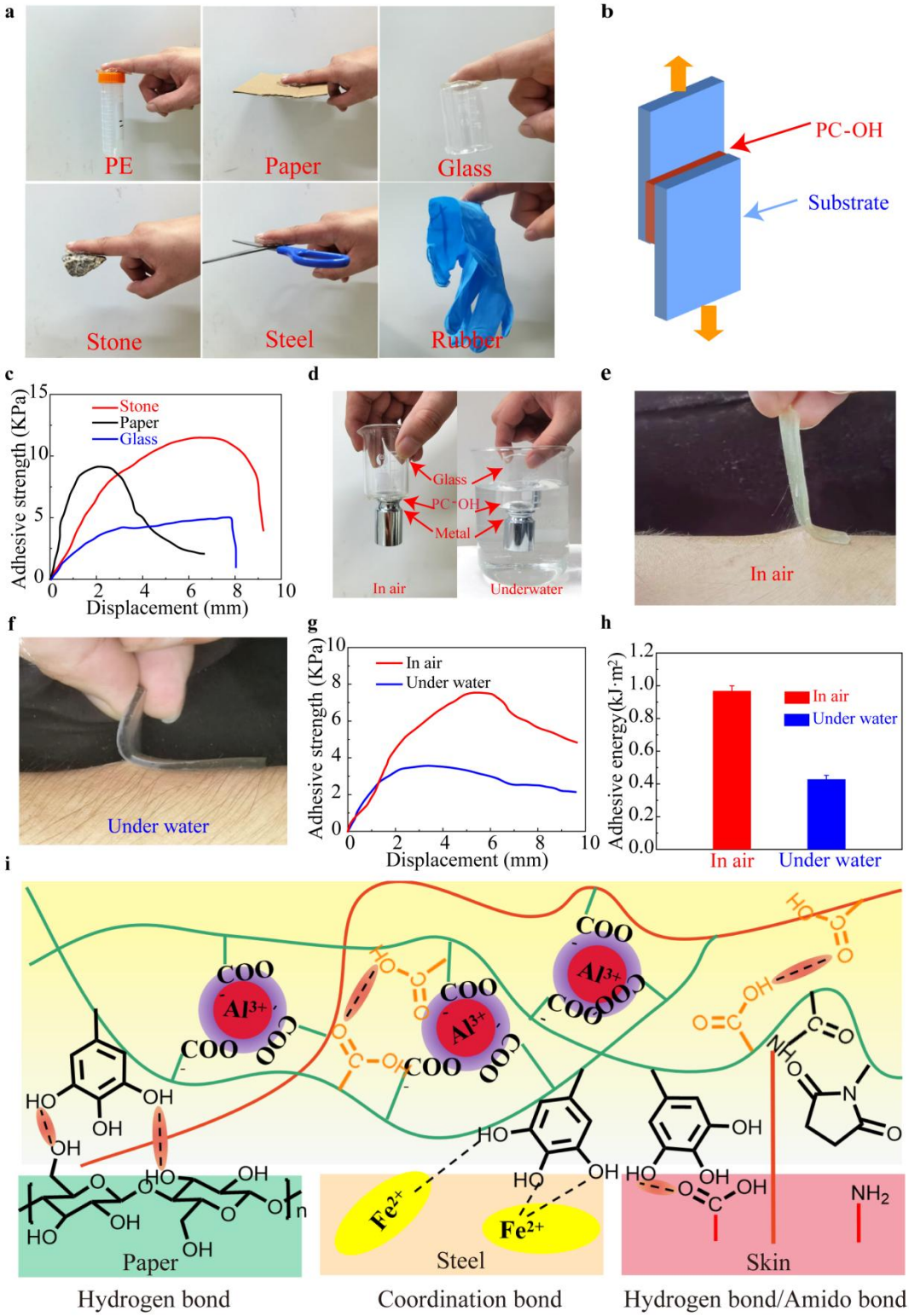

Fig. 5. Adhesive behaviors of the PC-OH organic hydrogel. Hydrogels can adhere to various substrate surfaces (plastic (pe), paper (cellulose), glass, stone, steel, and rubber) (a). Schematic illustration diagram of the lap shear test (b). The adhesive strength curves of lap shear tests on stone, paper (cellulose), glass, and porcine skin

glued by the PC-OH hydrogel (c). PC-OH organic hydrogel adhered to glass and metal and sustained adhesion in air and underwater (d). Photographs of PC-OH adhered to human skin in the air (e) and underwater (f). Adhesive strength (g) and adhesive energy (h) of PC-OH organic hydrogel adhered to pig skin in the air and underwater. Adhesion mechanism between the PC-OH and various substrates (wood (cellulose), metal (steel), and human skin) (h).

2.6 PC-OH touch strip

The potential of PC-OH for e-skin applications was investigated by applying PC-OH materials to 1D and 2D touch sensors. As shown in Fig. 6a, both ends of the 1D PC-OH touch strip were applied with in-phase alternating (AC) current through A1 and A2 current meters, and both are connected to copper (Cu) electrodes. When the 1D touch strip is touched by a human finger, in the interface of finger/PC-OH, the coupling capacitance (C_{finger}) can be generated, thus forming a closed-loop circuit, and then the current can flow through the human body to the ground.

Fig. 6b shows the equivalent circuit of the PC-OH 1D touch strip, and the strip is divided by the finger into two resistive parts. The touch strip position-sensing ability was also studied, as shown in Fig. 6c-e. The current flowing through the circuit varies with the touching position. The current magnitude relies on the parasitic capacitance generated baseline current, and the finger touch generated additional current.

The leakage current to the environment from the PC-OH touch panel generates the baseline current. When the PC-OH touch strip is touched with the finger, the additional current is generated as the current flows from the electrode to the grounded finger, as shown in Fig. 6d and e. As shown in Fig. 6e, The PC-OH strip was touched point by point by a finger from left to right (from $\alpha = 0.0$ - 1.0) with $\alpha = 0.2$ in steps, and the current was measured with A1 and A2 current meters. It can be seen that the total current I_t remains constant when the touch position changes from $\alpha = 0.0$ to 1.0, and the peak current decrease of I_1 is nearly linear, whereas the increase in the peak current of I_2 is nearly linear. This result shows that the touch current induced by the finger touch is proportional to the electrode-touch point distance, showing that the 1D

PC-OH touch strip has the touch position sensing ability. The 1D PC-OH touch strip exhibited stable performance with an extensive temperature range (-20 ~ 60°C). Fig. 6f-h shows the temperature change caused current variation of the PC-OH touch strip. The baseline currents are 3.83, 4.34, and 5.13 μA at -20, 25, and 60 °C. It can be seen that the conductivity of PC-OH increases, and the baseline current increases as the temperature increases. At the same time, finger touching generated additional current changes significantly with the temperature, e.g., the I_1 additional touch currents were 0.69, 0.99, and 1.31 μA at the position of α = 0.2 at -20, 25, and 60 °C. (Fig. 6f-h).

Furthermore, to investigate the effect of strain on the sensing response of the PC-OH touch strip, we stretched the 2D strip to twice the initial length, then touched it from the left (α = 0.0) to the right (α = 1.0) in steps of α = 0.2 point by point. In the stretched state, the PC-OH touch strip parasitic capacitance increased due to the touch strip/environment contact area expanding. As a result, the baseline current and the additional touch current increased simultaneously after stretching compared to the initial state (Fig. 6i). With the strip stretched, the baseline current increased from 4.34 μA to 7.36 μA. When a finger touches the stretched strip, an induced current is added to the baseline current. The touch current of the strip in the stretched state was 0.96 μA when touched with a finger at position α = 0.2, which was similar to the touch current in the undeformed state of 0.99 μA (currents were measured with the A1 current meter), showing that the current response of the touch strip is not influenced by stretching. The effect of wet environments (wet, dampish, and recovery) on the sensing response of the PC-OH touch strip was further investigated (Fig. 6j-p). The baseline currents of the electrode were 4.46, 4.39, and 4.35 μA, respectively. We can see that the baseline current increases sharply when the humidity increases because the contact area increases with the moisture. However, when touching the touch strip, the finger touch generated additional current increased only slightly with increasing moisture because the conductivity of PC-OH is essentially constant under these conditions, e.g., as shown in Fig. 6j-l, the additional touch currents of the electrodes are 1.53, 1.14, and 1.02 μA when touching the α = 0.2 position.

The localization ability of the finger touch position of the PC-OH touch strip can recover. As shown in Fig. 6q-t, two touch strips were cut (one is cut at α = 0.25, and the other is cut at both α = 0.25 and 0.75). The resulting strips are reconnected and healed after 5 min and 24 h. As shown in Fig. 6q and 6s, more significant current changes occur near the connected interface after cutting due to the interface's additional resistance (R_r and R_l). Also, with the self-healing time, the electronic self-healing efficiency increased while the additional resistances R_r and R_l decreased. In addition, comparing Fig. 6q and s (self-healed after 5 min), the baseline current and additional current of 2 cuts (Fig. 6s) were generally higher than 1 cut after self-healing (Fig. 6q) and from Fig. 6r and t (self-healed after 24 h), we can see that the two currents recorded after healing of 2 cuts were also higher than 1 cut which is because as the strip is cut and reconnected, the strip parasitic capacitance increases due to the increased touch strip/environment contact area. Therefore, the leakage current flows through the touch strip/environment-formed parasitic capacitance also increases. When α varies from 0.0 to 1.0, the output RMS currents difference of the touch strip is shown in Fig. 6u-w. The additional touch current has a linear negative relationship between the electrode/touch point distance. Therefore, using the RMS current to analyze the touch position can exclude the effects of strain, temperature, wetness, and damage on signal perception, indicating that the PC-OH touch strip has high operational stability and mechanical reliability under tensile conditions, wide temperature range (-20 ~ 60°C), wetness environment and damage conditions.

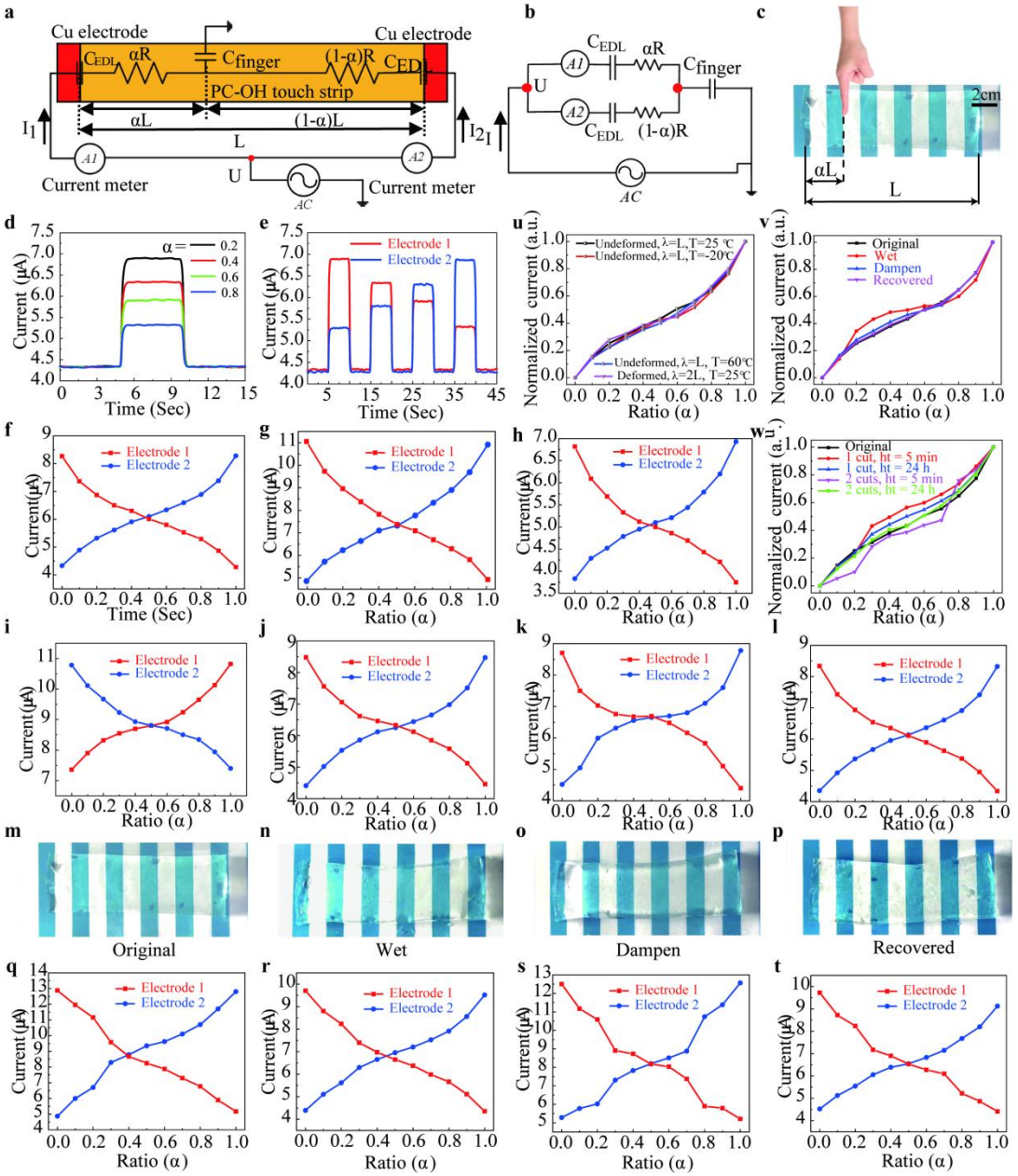

Fig. 6. The operating principle of the PC-OH touch strip (a) Schematic diagram of the 1D PC-OH touch strip. A closed circuit is formed when the finger touches the strip as the finger is grounded. (b) Schematic diagram of the electrical circuit of the PC-OH strip. (c) Schematic diagram showing the definition of the electrodes and 1D strip touch position, where L is the length of the touch strip, and αL is the distance from electrode A1 to the touch point. (d) A1 currents for different contact points (a = 0.2, 0.4, 0.6, and 0.8). When a finger touches the strip, additional touch current flows. Therefore, the A1 current magnitude decreases as the touch point moves far away from electrode A1. The current returns to the baseline value when the strip is no

longer in contact. (e) Currents measured from A1 and A2 at distances of α = 0.2, 0.4, 0.6, and 0.8 from the contact point to the A1 electrode during the contact period. A touch strip was tested at -20°C (f), 25°C (g), 60°C (h), and in the stretched state (λ = 2) (i). A touch strip was tested at different wet environments: wet (j), dampish (k), and recovery (j), and the photos of the touch strip were tested at different wet environments: original (m), wet (n), dampish (o), and recovery (p). A strip is tested by first cutting the touch strip and then reconnecting it at α = 0.25 and healing after 5 min (q) and 24 h (r). A touch strip is firstly tested by cutting it and then reconnecting it at α = 0.25 and 0.75 positions and healing after 5 min (s) and 24 h (t). The difference of the touch strip output current when α varies from 0.0 to 1.0 after stretching(λ=2) at 25, -20, 60, and 25℃ (u). The difference of the touch strip output current when α varies from 0.0 to 1.0 at different wet environments: original, wet, dampish, and recovery (v). When the touch position α was varied from 0.0 to 1.0, the difference of the touch panel output current in the original state and after the first cut, followed by joining at only at α = 0.25 position and at both α = 0.25 and 0.75 positions, and then healed after 5 min and 24 h, respectively (w).

2.7 2D PC-OH touch panel and wearable touch panel

The experiment was carried out on a 2D PC-OH touch panel to measure the touchpoint position (Fig. 7a-b and Supplementary Fig. 5 and 6). Four corners of the PC-OH film (2 mm thick) were connected to four copper electrodes, which were then connected to the same AC power source (±3V, 17kHz) by copper wires to ensure the voltage applied on the four corners was the same in magnitude and phase. The current meters A1, A2, A3, and A4 were between the power source and each electrode. α and β are two normalized distances that can be used to describe the touchpoint on the panel, as shown in Fig. 7a. The corresponding position at the lower left corner of the touch panel is (α, β) = (0, 0), while the corresponding position at the upper right corner is (α, β) = (1, 1). Four virtual resistive parts are formed by touching various points with a finger, separating the touch panel. Each virtual resistor was connected in

series with an electric double-layer capacitor (C_{EDL}) and a current meter in the circuit. The four parts were connected in parallel, which was then connected in series with the coupling capacitance (C_{finger}), which formed at the finger/PC-OH interface (Fig. 7b). Four representative touchpoints TP#1 (0.25, 0.75), TP#2 (0.75, 0.75), TP#3 (0.75, 0.25), and TP#4 (0.25, 0.25) were tested. When the finger successively touches these touchpoints, the currents detected by the four current meters installed in each corner were recorded.

Fig. 7c-e shows the measured currents when touching the four representative touchpoints (TP#1, TP#2, TP#3, and TP#4) in turn at different temperatures (-20, 25, and 60°C). As can be seen from the results, the corresponding additional touch current decreases when the finger moves far away from the end of the strip. For example, at 25°C (Fig. 7c), when the finger touched the position from TP#1 to TP#2, the I_1 current decreased from 5.25μA to 1.32μA. Then, when the touch position changed from TP#2 to TP#3, the I_1 current decreased from 1.32 to 0.79μA. On the other hand, when the touch position changed from TP#3 to TP#4, the I_1 current increased from 0.79 to 1.31μA. In addition, for a given touchpoint, the touch currents are inversely proportional to the corresponding distance from the finger touch point to the end of the touch strip. For example, the A1, A2, A3, and A4 currents at TP#1 are 11.41, 7.48, 6.76, and 7.67 μA at 25°C, respectively (Fig. 7c), corresponding to additional touch currents of 5.25, 1.31, 0.97, and 1.28 μA for I_1, I_2, I_3, and I_4, respectively (Fig. 7c). This is consistent with the normalized positions α and β of 0.26 and 0.74 for TP#1, respectively (Supplementary Table 1). As shown in Figs. 7c-e, the output positions match well with the input positions at different temperatures (-20°C, 25°C, 60°C), indicating that we can use the 2D PC-OH touch panel to detect the finger contact positions over an extensive temperature range (-20~60°C).

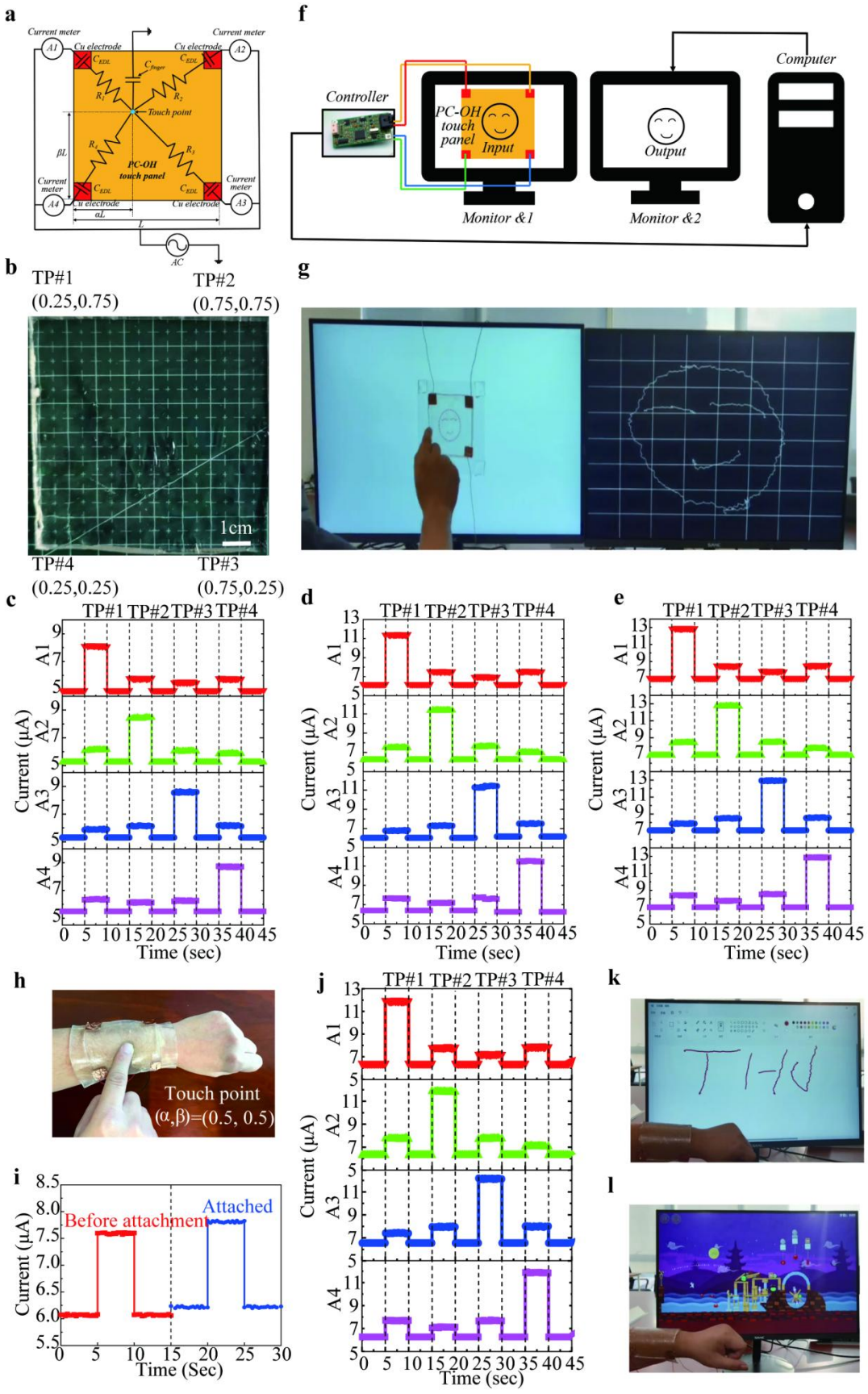
a
Current meter
Cu electrode
Touch point
PC-OH touch panel
f
Controller
PC-OH touch panel
Input
Output
Computer
Monitor &1
Monitor &2
b
TP#1 (0.25,0.75)
TP#2 (0.75,0.75)
TP#4 (0.25,0.25)
TP#3 (0.75,0.25)
1cm
g
c
d
e
TP#1 TP#2 TP#3 TP#4
Current (μA)
Time (sec)
h
Touch point
(α,β)=(0.5, 0.5)
i
Before attachment
Attached
Time (Sec)
j
k
l

Fig. 7. Position sensing and operation of a 2D PC-OH touch panel. (a) The illustration of the PC-OH touch panel, where α and β represent the two normalized distances of the touch position. (b) Optical photograph of the transparent PC-OH touch panel. The sensitivity of position detection can be seen by studying the panel's four touchpoints (TP#1 ~ TP#4). By touching TP#1 ~ TP#4 successively, and using four current meters A1, A2, A3, and A4 to measure the change in currents I1, I2, I3, and I4 with time at different temperatures of -20°C (c), 25°C (d), and 60°C (e). (f) The touch panel is integrated with a desktop through a control board to form a touch system. (g) The function of the touch panel is detected by drawing a smiling face. (h) The touch panel is attached to the human arm. (i) The A1 current of the panel before and after the arm attachment is recorded. (j) The position sensitivity after attachment is studied by measuring A1, A2, A3, and A4 currents at different touch points. The wearable touch panel can detect actions such as clicking, holding, dragging, and swiping. The ability of the touch panel for writing text (k) and playing computer games (l) was demonstrated.

A square PC-OH panel adheres to a larger square PMMA board, and then the other side of the PMMA board is fixed to the display to achieve electrical insulation of the PC-OH panel. Copper electrodes are attached to the four corners of the PC-OH and then connected to the same control board to generate the same phase AC current (±3 V, 17 kHz) at each corner. The control board measures the current at each corner by converting the real-time currents of I_1, I_2, I_3, and I_4 into digital signals, which are then transmitted to the computer when the touch panel is touched by a finger (Fig. 7f). The coordinates of the finger's touch position can be calculated by the computer and display it on the screen. Therefore, it is possible to touch the touch panel and display the corresponding touching point simultaneously. A smiling face and concentric square were drawn on the integrated touch panel (Fig. 7g and Supplementary Movie 2 and 3), and we can see some distortion at the edges of the output image of the running man due to the nonlinearity of the 2D touch panel resistances. The touch panel can also be used in wet environments (Supplementary Movie 4). For example, after

pouring water on the touch panel, a nearly identical concentric circle can be drawn on the touch screen by tracing the pattern behind the PC-OH. In addition, the touch panel has a self-healing ability. A concentric circle was drawn on the touch panel by tracing the pattern behind the PC-OH, and then we cut a crack on the PC-OH, and the resulting pieces were reconnected for healing. After 24 hours of healing, a nearly identical concentric circle pattern was successfully drawn again by drawing the same pattern again (Supplementary Movies 5 and 6). The results show that the PC-OH touch panel has high operational reliability and mechanical flexibility under ultra-high stretch states, wide temperature range (-20~60°C), wet environments, and damaged states

Then A wearable touch panel was developed based on the 2D PC-OH touch panel sensing mechanism. The PC-OH touch panel was insulated from the human skin by attaching a 2.0 mm thick PC-OH film to a 1.0 mm thick highly bonded (VHB) film (Fig. 7h). Copper electrodes were attached to each corner of the PC-OH touch panel and then connected to the computer. The wearable touch panel is transparent, soft, and stretchable, making it comfortable to wear on the body while transmitting the touch panel's optical information. The measured currents are compared before and after attaching the wearable touch panel to the human arm (Fig. 7i). The results show a slight increase in the baseline current (from 1 μA to 2 μA) due to the leakage current flowing from the touch panel to the human body through the VHB substrate. Then, touchpoints TP#1 to TP#4 on the wearable touch panel were touched successively, and the current meters measured the A1, A2, A3, and A4 currents in real time. The results show that the correlation between the measured currents and touch positions was not affected by the attachment (Fig. 7j). The results show that the wearable touch panel was able to successfully sense various motions like tapping, holding, dragging, or swiping, when the finger touched the touch panel, and could be worn on the human body to write texts (Fig. 7k and Supplementary Movie 7), draw figures (Supplementary Fig. 27 and Supplementary Movie 8), and play games (Fig. 7l and Supplementary Movie 9).

3. Discussion

In summary, our gelatin-PAA-based hydrogel (PC-OH) is a highly versatile material that possesses several key properties, including high optical transparency, good ionic conductivity, high stretchability, autonomous self-healing ability, and strong self-adhesive ability in both air and water. These unique features make it an attractive material for a wide range of applications in fields such as electronics, biomedical engineering, and robotics. We demonstrated the potential of PC-OH as an electrode material by developing a highly stretchable, transparent, and self-healing touch panel based on a surface capacitive touch (SCT) system. In this system, the detected current accurately reflects the position of the finger on the PC-OH touch panel, making it suitable for a variety of position-sensing applications. We investigated the position-sensing mechanism of the PC-OH touch panel with a 1D touch strip, which showed accurate and fast touch sensing even in self-healing and highly stretchable states, as well as in different temperatures and wet environments. Furthermore, we extended the position sensing capability to 2D PC-OH touch panels by connecting them to a computer, allowing for a range of human-computer interactions in real-world applications based on its detection ability. The touch panel can be used for various activities such as writing, drawing, and playing computer games, making it a promising candidate for next-generation touchscreens. Overall, the development of PC-OH hydrogel touch panels has the potential to revolutionize the field of human-machine interaction by enabling the creation of more natural, flexible, and responsive interfaces that can adapt to changing environments and be seamlessly integrated into our daily lives.

CRediT authorship contribution statement

Conceptualization: Zhenglin Chen, Jiaqi Yang, Dongmei Yu, Peiwu Qin, Can Yang Zhang.

Methodology: Zhenglin Chen, Likun Zhang, Zhengyang Lei, Canhui Yang, Ying Zhu.

Investigation: Zhenglin Chen, Qianhui Sun, Lulu Xu.

Visualization: Zhenglin Chen, Ziheng Zhang, Xiaopeng Zhang.

Supervision: Dongmei Yu, Peiwu Qin, Can Yang Zhang.

Writing—original draft: Zhenglin chen, Jiaqi Yang, Likun Zhang, Zhengyang Lei, Canhui Yang, Ying Zhu, Haifei Guan, Qianhui Sun, Lulu Xu, Hao Zhang, Ziheng Zhang, Sen Zeng, Chuhui Wang, Rongxu Yan, Peter E Lobie.

Writing—review & editing: Zhenglin chen, Dongmei Yu, Peiwu Qin, Can Yang Zhang.

Declaration of competing interest

The authors declare that they have no competing interests. The authors claim that none of the material in the paper has been published or is under consideration for publication elsewhere. All authors have seen the manuscript and approved to submit to your journal.

Acknowledgments

We thank the support from the National Natural Science Foundation of China (31970752,22278242), China Postdoctoral Science Foundation (2023M730856), Shenzhen excellent scientific and technological innovation talent training program (RCBS20221008093129082), Science, Technology, Innovation Commission of Shenzhen Municipality (JCYJ20190809180003689, JSGG20200225150707332, JCYJ20220530143014032, KCXFZ20211020163813019, ZDSYS20200820165400003, WDZC20200820173710001, WDZC20200821150704001, JSGG20191129110812708), Shenzhen Bay Laboratory Open Funding (SZBL2020090501004, SZBL2021080601011), Department of Chemical Engineering-iBHE special cooperation joint fund project (DCE-iBHE-

2022-3), Tsinghua Shenzhen International Graduate School Cross-disciplinary Research and Innovation Fund Research Plan (JC2022009), Bureau of Planning, Land and Resources of Shenzhen Municipality (2022-207).

References:

[1] *X. Guo, F. Yang, X. Sun, Y. Bai, G. Liu, W. Liu, R. Wang, X. He,* Adv Funct Mater ***2022***, 32, *2201230.*

[2] *C. Han, F. Yang, X. Guo, Y. Bai, G. Liu, H. Sun, P. Wang, W. Liu, R. Wang,* Adv Mater Interfaces ***2021***, 8, *2100742.*

[3] *C. C. Kim, H. H. Lee, K. H. Oh, J. Y. Sun,* Science (1979) ***2016***, 353, *682.*

[4] *G. Gao, F. Yang, F. Zhou, J. He, W. Lu, P. Xiao, H. Yan, C. Pan, T. Chen, Z. L. Wang,* Advanced Materials ***2020***, 32, *2004290.*

[5] *Z. Chen, F. Li, L. Zhang, Z. Lei, C. Yang, C. Xiao, L. Lian, X. Yuan, G. Ijaz, J. Yang, Z. Lin, Y. He, P. Zhang, D. Yu, P. Qin,* Chemical Engineering Journal ***2023***, 451, *138672.*

[6] *X. Guo, F. Yang, W. Liu, C. Han, Y. Bai, X. Sun, L. Hao, W. Jiao, R. Wang,* J Mater Chem A Mater ***2021***, 9, *14806.*

[7] *B.-J. Cheon, J.-W. Kim, M.-C. Oh,* Opt Express ***2013***, 21, *4734.*

[8] *Y. Zhang, L. Chen, C. Yan, P. Qin, X. Ji, Q. Dai,* IEEE Transactions on Circuits and Systems for Video Technology ***2018***, 30, *11.*

[9] *M. Takasaki, H. Kotani, T. Mizuno, T. Nara, in* 2005 IEEE/RSJ International Conference on Intelligent Robots and Systems, IROS, *IEEE, **2005**, pp. 3354–3359.*

[10] *M. C. Brenner, J. J. Fitzgibbon,* J Acoust Soc Am ***1988***, 84, *1578.*

[11] *H. Hoshyarmanesh, N. Nehzat, M. Salehi, M. Ghodsi, H. S. Lee, H. H. Park,* Materials and Manufacturing Processes ***2014***, 29, *870.*

[12] *Z. Cui, A. Huang, J. Chen, S. Gao,* IEEE Sens J ***2021***, 21, *26389.*

[13] *H. Park, S. J. Oh, D. Kim, M. Kim, C. Lee, H. Joo, I. Woo, J. W. Bae, J. H. Lee,* Advanced Science ***2022***, 9, *2201070.*

[14] *Y. Lee, S. Lim, W. J. Song, S. Lee, S. J. Yoon, J. M. Park, M. G. Lee, Y. L. Park, J. Y. Sun,* Advanced Materials ***2022***, 34, *2108586.*

[15] *Z. Chen, B. Cotterell, W. Wang,* Eng Fract Mech ***2002***, 69, *597.*

[16] *S. Yang, E. Ng, N. Lu,* Extreme Mech Lett ***2015***, 2, *37.*

[17] *S. Yoon, Y. J. Kim, Y. R. Lee, N. E. Lee, Y. Won, S. Gandla, S. Kim, H. K. Kim,* NPG Asia Mater ***2021***, 13, *1.*

[18] *K. McLellan, Y. Yoon, S. N. Leung, S. H. Ko,* Adv Mater Technol ***2020***, 5, *1900939.*

[19] *C. Ma, H. Luo, M. Liu, H. Yang, H. Liu, X. Zhang, L. Jiang,* Chemical Engineering Journal ***2021***, 425, *131542.*

[20] *H. Yu, Y. Tian, M. Dirican, D. Fang, C. Yan, J. Xie, D. Jia, Y. Liu, C. Li, M. Cui, H. Liu, G. Chen, X. Zhang, J. Tao,* Carbohydr Polym ***2021***, 273, *118539.*

[21] *Y. Yan, L. Wei, X. Qiu, J. Shao, H. Liu, X. Cui, J. Huang, L. Xie, Z. Hu, C. Huang,* ACS Appl Polym Mater ***2021***, 3, *1479.*

[22] *M. Bahri, M. A. Elaguech, S. Nasraoui, K. Djebbi, O. Kanoun, P. Qin, C. Tlili, D. Wang,* Microchemical Journal ***2023***, 185, *108208.*

[23] *Y. W. Lee, S. Chun, D. Son, X. Hu, M. Schneider, M. Sitti,* Advanced Materials ***2022***, 34, *2109325.*

[24] *B. Grigoryan, S. J. Paulsen, D. C. Corbett, D. W. Sazer, C. L. Fortin, A. J. Zaita, P. T. Greenfield, N. J. Calafat, J. P. Gounley, A. H. Ta, F. Johansson, A. Randles, J. E. Rosenkrantz, J. D. Louis-Rosenberg, P. A. Galie, K. R. Stevens, J. S. Miller,* Science (1979) ***2019***, 364, *458.*

[25] *H. Zhang, H. Xu, W. Sun, X. Fang, P. Qin, J. Huang, J. Fang, F. Lin, C. Xiong,* Acta Biomater ***2023***, 159, *38.*
[26] *V. M. Kadiri, C. Bussi, A. W. Holle, K. Son, H. Kwon, G. Schütz, M. G. Gutierrez, P. Fischer,* Advanced Materials ***2020***, 32, *2001114.*
[27] *G. Khandelwal, T. Minocha, S. K. Yadav, A. Chandrasekhar, N. P. M. J. Raj, S. C. Gupta, S.-J. Kim,* Nano Energy ***2019***, 65, *104016.*
[28] *Q. Chen, I. Gul, C. Liu, Z. Lei, X. Li, M. A. Raheem, Q. He, Z. Haihui, E. Leeansyah, C. Y. Zhang,* J Med Virol ***2023***, 95, *e28385.*
[29] *D. Fan, X. Yuan, W. Wu, R. Zhu, X. Yang, Y. Liao, Y. Ma, C. Xiao, C. Chen, C. Liu,* Nat Commun ***n.d.***
[30] *R. Guo, Y. Fang, Z. Wang, A. Libanori, X. Xiao, D. Wan, X. Cui, S. Sang, W. Zhang, H. Zhang, J. Chen,* Adv Funct Mater ***2022***, 32, *2204803.*
[31] *Y. Wang, Y. Xia, P. Xiang, Y. Dai, Y. Gao, H. Xu, J. Yu, G. Gao, K. Chen,* Chemical Engineering Journal ***2022***, 428, *131171.*
[32] *A. Beck, F. Obst, D. Gruner, A. Voigt, P. J. Mehner, S. Gruenzner, R. Koerbitz, M. H. Shahadha, A. Kutscher, G. Paschew, U. Marschner, A. Richter,* Adv Mater Technol ***2022***, *2200417.*
[33] *Y. Zhang, C. K. Jeong, J. Wang, X. Chen, K. H. Choi, L. Q. Chen, W. Chen, Q. M. Zhang, Q. Wang,* Advanced Materials ***2021***, 33, *2103056.*
[34] *Z. Xu, F. Zhou, H. Yan, G. Gao, H. Li, R. Li, T. Chen,* Nano Energy ***2021***, 90, *106614.*
[35] *H. Dinh Xuan, B. Timothy, H. Y. Park, T. N. Lam, D. Kim, Y. Go, J. Kim, Y. Lee, S. Il Ahn, S. H. Jin, J. Yoon,* Advanced Materials ***2021***, 33, *2008849.*
[36] *B. Yang, Y. Zhao, M. U. Ali, J. Ji, H. Yan, C. Zhao, Y. Cai, C. Zhang, H. Meng,* Advanced Materials ***2022***, 34, *2201342.*
[37] *Z. Jiang, P. Song,* Science (1979) ***2022***, 376, *245.*
[38] *C. Y. Lo, Y. Zhao, C. Kim, Y. Alsaid, R. Khodambashi, M. Peet, R. Fisher, H. Marvi, S. Berman, D. Aukes, X. He,* Materials Today ***2021***, 50, *35.*
[39] *K. Cho, D. Kang, H. Lee, W. G. Koh,* Chemical Engineering Journal ***2022***, 427, *130879.*
[40] *D. Fan, X. Yuan, W. Wu, R. Zhu, X. Yang, Y. Liao, Y. Ma, C. Xiao, C. Chen, C. Liu, H. Wang, P. Qin,* Nat Commun ***2022***, 13, *5083.*
[41] *Z. Zhang, Z. Yao, Y. Li, S. Lu, X. Wu, Z. Jiang,* Chemical Engineering Journal ***2022***, 433, *134488.*
[42] *A. Heiden, D. Preninger, L. Lehner, M. Baumgartner, M. Drack, E. Woritzka, D. Schiller, R. Gerstmayr, F. Hartmann, M. Kaltenbrunner,* Sci Robot ***2022***, 7, *eabk2119.*
[43] *Y. Xu, Q. Rong, T. Zhao, M. Liu,* Giant ***2020***, 2, *100014.*
[44] *Y. Niu, H. Liu, R. He, M. Luo, M. Shu, F. Xu,* Small ***2021***, 17, *2101151.*
[45] *X. Zhang, C. Cui, S. Chen, L. Meng, H. Zhao, F. Xu, J. Yang,* Chemistry of Materials ***2022***, 34, *1065.*
[46] *B. Ying, R. Z. Chen, R. Zuo, J. Li, X. Liu,* Adv Funct Mater ***2021***, 31, *2104665.*
[47] *X. Sui, H. Guo, C. Cai, Q. Li, C. Wen, X. Zhang, X. Wang, J. Yang, L. Zhang,* Chemical Engineering Journal ***2021***, 419, *129478.*
[48] *J. Wang, Y. Huang, B. Liu, Z. Li, J. Zhang, G. Yang, P. Hiralal, S. Jin, H. Zhou,* Energy Storage Mater ***2021***, 41, *599.*

[49] *Y. Chen, X. Guo, A. Mensah, Q. Wang, Q. Wei,* ACS Appl Mater Interfaces ***2021***, 13, *59761*.
[50] *M. Guo, X. Yang, J. Yan, Z. An, L. Wang, Y. Wu, C. Zhao, D. Xiang, H. Li, Z. Li, H. Zhou,* J Mater Chem A Mater ***2022***, 10, *16095*.
[51] *C. Lu, J. Qiu, W. Zhao, E. Sakai, G. Zhang, R. Nobe, M. Kudo, T. Komiyama,* Int J Biol Macromol ***2021***, 188, *534*.
[52] *L. J. Hawkins, M. Wang, B. Zhang, Q. Xiao, H. Wang, K. B. Storey,* Comp Biochem Physiol Part D Genomics Proteomics ***2019***, 30, *1*.
[53] *X. F. Zhang, X. Ma, T. Hou, K. Guo, J. Yin, Z. Wang, L. Shu, M. He, J. Yao,* Angewandte Chemie - International Edition ***2019***, 58, *7366*.
[54] *Y. Feng, J. Yu, D. Sun, W. Ren, C. Shao, R. Sun,* Chemical Engineering Journal ***2022***, 433, *133202*.
[55] *P. Shi, Y. Wang, W. W. Tjiu, C. Zhang, T. Liu,* ACS Appl Mater Interfaces ***2021***, 13, *49358*.
[56] *C. Xie, X. Wang, H. He, Y. Ding, X. Lu,* Adv Funct Mater ***2020***, 30, *1909954*.
[57] *E. Wieschaus, R. Riggleman,* Cell ***1987***, 49, *177*.
[58] *C. Capitain, S. Wagner, J. Hummel, N. Tippkötter,* Waste Biomass Valorization ***2021***, 12, *1761*.
[59] *A. V. S. Sarma, A. Anbanandam, A. Kelm, R. Mehra-Chaudhary, Y. Wei, P. Qin, Y. Lee, M. V Berjanskii, J. A. Mick, L. J. Beamer,* Biochemistry ***2012***, 51, *807*.
[60] *H. J. Kim, H. L. Choi, Y. S. Ahn,* J Alloys Compd ***2019***, 805, *648*.

Supporting Information

Biocompatible wearable touch panel based on ionically conductive organic hydrogels with anti-freezing, anti-dehydration, self-healing, and underwater adhesion properties

Zhenglin Chen[a, b], Jiaqi Yang[c], Likun Zhang[a, b], Haifei Guan[a, b], Zhengyang Lei[a, b], Xiaopeng Zhang[a], Canhui Yang[d], Ying Zhu[a, b], Qianhui Sun[a, b], Lulu Xu[a, b], Ziheng Zhang[a, b], Sen Zeng[a, b], Chuhui Wang[a, b], Rongxu Yan[a, b], Chong Zhang[e, f], Peter E Lobie[a, b, g], Dongmei Yu[h, *], Peiwu Qin[a, b, *], and Can Yang Zhang[a, b, e, *]

[a]Center of Precision Medicine and Healthcare, Tsinghua-Berkeley Shenzhen Institute, Shenzhen, Guangdong Province, 518055, China

[b]Institute of Biopharmaceutics and Health Engineering, Tsinghua Shenzhen International Graduate School, Shenzhen, Guangdong Province, 518055, China

[c]State Key Laboratory of Urban Water Resources and Environment, School of Civil & Environmental Engineering, Harbin Institute of Technology (Shenzhen), Shenzhen, Guangdong 518055, China

[d]Soft Mechanics Lab, Department of Mechanics and Aerospace Engineering, Southern University of Science and Technology, Shenzhen, Guangdong 518055, China

[e]MOE Key Laboratory for Industrial Biocatalysis, Institute of Biochemical Engineering, Department of Chemical Engineering, Tsinghua University, Beijing 100084, China

[f]Center for Synthetic and Systems Biology, Tsinghua University, Beijing 100084, China

[g]Shenzhen Bay Laboratory, Shenzhen, Guangdong 518055, China.

[h]School of Mechanical, Electrical & Information Engineering, Shandong University, Weihai, Shandong 264209, China

Z. Chen, J. Yang, and L. Zhang contributed equally to this work.

* Corresponding authors E-mail address: yudongmei@sdu.edu.cn (D. Yu), pwqin@sz.tsinghua.edu.cn (P. Qin), zhang.cy@sz.tsinghua.edu.cn (C.Y. Zhang).

Methods and Materials

Materials: Gelatin (≥99.5%, ~250 g Bloom), acrylic acid n-hydroxysuccinimide ester (AA-NHS, ≥90 %), tannic acid (TA, 95%), aluminum chloride hexahydrate ($AlCl_3 \cdot H_6O_2$, 99.99%) and α-ketoglutaric acid (98%) were purchased from the Aladdin Industrial Corporation (Shanghai, China). Acrylic acid N-hydroxysuccinimide ester (AA-NHS ester, ≥90%) and gelatin methacrylate (GelMA; bloom 250; degree of substitution (DS) 60%) were purchased from Sigma-Aldrich (Shanghai, China). Glycerol (≥99.5%) was purchased from General Reagent (Shanghai, China). All materials were used as received without further purification. Milli-Q (18.2 MΩ cm^{-1}) was used for all experiments.

Preparation of PC-OH: P (AA-co-AAm, PC) based organohydrogel (PC-OH) was synthesized via three steps. The first step is the preparation of the precursor solution. Briefly, gelatin (10% (w/w)), acrylic acid (30% (w/w)), AA-NHS ester (1% (w/w)), TA (0.15% (w/w)), $AlCl_3 \cdot H_6O_2$ (3% (w/w)), α-ketoglutaric acid (0.4% (w/w)), and GelMA (0.1% (w/w)) were added in Milli-Q water (MΩ·cm) to acquire the precursor solution. The solution was mixed with a magnetic stirrer at 65 °C for 2 h to make the prepolymer solution dispersed evenly. The next step is the curing of the precursor solution. The clarified mixture solution was poured into two rectangular poly (methyl methacrylate) (PMMA) molds (length: 100.0 mm; width: 100.0 mm; and thickness: 1.0 mm) separated by silicone pieces (height = 2.0 mm) and then cooled for 30 min. Subsequently, the mold was put into a UV chamber with an intensity of 10 mW/cm^2 for photopolymerization within 40 min to cure thoroughly to obtain the gelatin-PAA-based hydrogel (PC-H). The final step is the immersion in an ionic solution, Gelatin-PAA-based organic hydrogel (PC-OH) was prepared by immersing the obtained PC-H in Milli-Q water/glycerol binary solvent (1:1 (v/v)) for 4 hours.

Similarly, a PC-based hydrogel (PC-H) precursor solution could be prepared by adding the above solutes into Milli-Q water (MΩ·cm). The solution was mixed with a magnetic stirrer at 65 °C for 2 h to make the prepolymer solution dispersed evenly. Next, the clarified mixture solution was poured into two rectangular poly (methyl methacrylate) (PMMA) molds (length: 100.0 mm; width: 100.0 mm; and thickness:

1.0 mm) separated by silicone pieces (height = 2.0 mm) and then cooled for 30 min. Subsequently, the mold was put into a UV chamber with an intensity of 10 mW/cm^2 for photopolymerization within 40 min to cure thoroughly to obtain the PAA-based hydrogel (PA-H). Finally, PAA-based organic hydrogel (PA-OH) was prepared by immersing the obtained PA-H in Milli-Q water/glycerol binary solvent (1:1 (v/v)) for 4 hours.

Characterizations: To characterize the properties of organic hydrogel (PC-OH), the gels were freeze-dried. Then the microstructure photos and infrared spectra were collected by SEM (GeminiSEM 50, Zeiss) and FTIR spectrometer (iS50, Nicolet) using the attenuated total reflectance (ATR) method in the spectral range of 4000-400 cm^{-1}, respectively. The anti-freezing performance of gels was tested by differential scanning calorimetry (TGA/DSC 2, Mettler-Toledo), with a heating rate of 5 °C min^{-1} in the temperature range of –60 ~ 60 °C under air atmosphere. UV-Vis-NIR spectrophotometer (Cary 5000, Agilent) was used to measure the transmittance of the gel samples with a wavelength range from 400 to 800 nm. The anti-dehydration tests were conducted at 25 °C and 60% relative humidity (RH), the thickness of the gel samples is 2.0 mm, and the air is the reference for measuring transparency. To characterize the environmental stability of PC-OH organic hydrogel, the relative humidity of the humidity-controlled cabinet is controlled at 38%, and the temperature is set to 25 °C. all samples are cut to initial sizes of 40.0 × 20.0 × 2.0 mm. The sample weight was measured once a day for 7 consecutive days using an electronic scale. The remaining weight ratios of samples were calculated according to the m/m_0 formula, where m_0 is the original weight of the gel samples and m is the weight of gel samples after being stored for specific days.

Electromechanical properties: Digital photographs were taken with a camera (Nikon D90) of samples subjected to various mechanical deformations (including stretching, bending, and twisting) after being stored at different conditions (-20°C, 25°C, and 60°C) for 24 hours. The tensile tests are operated on a tension testing machine system (5985, Instron). The strip samples (40.0 × 20.0 × 2.0 mm) with a crosshead distance of 5.0 mm were stretched at a constant speed of 30.0 mm min^{-1}.

The samples were stored at -20 ◦C, 25 ◦C, or 60 ◦C for at least 24 h before testing. To conduct the low-temperature tests, we placed a -20 °C cooling chamber around the sample to keep the whole sample at -20 °C during the stretching process. Similarly, to conduct high-temperature tests, we placed a heating chamber around the sample to keep the whole sample at 60 °C during the stretching process. The slope of the stress-strain curve in the strain range of 0% to 10% is used to determine the modulus of the samples. The strain is calculated as $\varepsilon=(l-l_0)/l_0 \times 100\%$, where l_0 is the initial gauge length, and l is the length after deformation. The tensile stress σ can be calculated by $\sigma = F/A_0$, where A_0 is the initial cross-sectional area and F is the tensile load.

The ionic conductivities of the materials are obtained from the complex impedance plots measured by an electrochemical workstation (PARSTAT 4000A, Princeton) in the frequency range of 0.1 Hz to 1 MHz with an alternating-current sine wave amplitude of 200 mV. The PC-OH sample is cut into a cylindrical shape (diameter: 12.0 mm, depth: 2.0 mm) and sandwiched between two round steel electrodes. The materials' bulk resistance (R_b) is obtained by fitting the intercept of the real axis of the Nyquist plot at a high frequency using the Z-view software. The conductivity of the stretchable PC-OH is calculated by $\sigma = L/(A \cdot R_b)$, where L corresponds to the distance between the electrodes, and A denotes the cross-sectional area of the sample.

Adhesive Test: The lap shear test was conducted to study the adhesion property of PC-OH organic hydrogel on the interface between various substrate surfaces (plastic, paper, glass, stone, steel, and rubber) and the PC-OH organic hydrogel. Besides, to study the adhesion performance of the PC-OH organic hydrogel more accurately, the rectangular PC-OH organic hydrogel (30.0 mm × 30.0 mm × 2.0 mm) was attached between the surfaces of two substrates. Afterward, the samples were pulled at a fixed speed of 10.0 mm min^{-1} until separation by a tensile machine (5985, Instron) under ambient conditions. As can be seen from the displacement-force curve, the measured force reaches a plateau value after the peeling process enters a steady state, and the adhesive strength can be calculated by dividing the maximum load by the initial adhesion area. The adhesion energy can be calculated by dividing two times the plateau force by the width of the specimen. To further characterize the adhesion

performance of PC-OH under different conditions, adhered specimens were subjected to lap shear tests at different temperatures (e.g., a subzero temperature of -20°C, room temperature of 25°C and high temperature of 60°C) and humid environments (underwater). In these tests, polyethylene terephthalate (PET) films and cyanoacrylate adhesives were used as stiff backing and substrates for PC-OH organic hydrogels.

Self-healing tests: Before testing, the samples are stored at a determined temperature (–20, 25, or 60 ℃) for at least 12 h. To study the mechanical properties of the self-healed PC-OH organic hydrogel, the samples are cut into two pieces, and then the sections are joined together and stored for at least 24 hours for self-healing. The mechanical properties of the self-healed sample are then tested with a universal material testing machine (5985, Instron). Using an optical microscope (BX 53, Olympus) to study the time-dependent self-healing process, the samples are cut with a sharp knife and then gently joined together the cut surfaces in the air. To measure the before and after self-healing direct current (DC) of the PC-OH sample, a PC-OH strip (4.0 × 2.0 × 0.1 cm) is connected to a current meter (Model 34461A, Agilent). A DC voltage of 3.0 V is applied to the PC-OH strip using a function generator (Model 33612A, Agilent). The touch strip is cut into two pieces with a sharp ceramic knife, and then the two sections are joined together, and the currents are recorded with time in the whole process.

Biocompatibility test in vitro: In vitro biocompatibility testing of PC-OH was performed by the 3-(4,5-dimethylthiazol-2-yl)-2,5-diphenyltetrazolium bromide (MTT) assay (CCK-8 kit, Yeasen, Guangzhou, China). WST-8 (2-(2-methoxy-4-nitrophenyl)-3-(4-nitrophenyl)-5-(2,4-disulfophenyl)-2H-tetrazolium monosodium salt) can be reduced by mitochondrial dehydrogenase in the presence of the electron-coupled carrier 1-METHOXY PMS to produce a highly water-soluble orange-yellow methanogenic product (FORMAZAN), the color shade of which is proportional to the proliferation of cells The color is proportional to cell proliferation and inversely proportional to cytotoxicity. The OD value was measured at 450 nm using an enzyme marker to reflect the number of viable cells indirectly. In this work, a piece of PC-OH organic hydrogel (2.0 g) was immersed in 10 mL of deionized water for 24 h at room

temperature. Then A549 cells were plated in a 96-well plate (2000 cells/well) with six parallel Wells (n=6) in which A549 cells were cultured in Dulbecco's Modified Eagle Medium (DMEM) medium (HyClone, USA) and complete growth medium with 10% fetal bovine serum, 100 U mL^{-1} penicillin and 0.1 mg mL^{-1} streptomycin (Thermo Fisher Scientific, USA) at 37 ° C in 5% CO^2. The total volume of the medium used in this work was 100uL. After 12h of cell culture, 100 μL PC-OH organic hydrogel extract was added to the medium, and the cells were then incubated at 37℃ for 24 h, 48 h, and 72 h. At the time point to be measured, CCK-8 (10 μL), 10% of the total volume of the medium, was added and incubated for 2h in the dark, after which optical density was measured at 450 nm using a microplate reader (Tecan MicroplateReader Spark, USA). Here, for fluorescence imaging, cells were incubated with PC-OH hydrogel extract for 24 h, then stained with 2 μg mL^{-1} Calcein-AM (Biolab, China), incubated in the dark for 30min in an incubator, and then washed three times with PBS. After adding the medium, the images were taken with a confocal fluorescence microscope (Nikon A1R SI confocal, Japan).

In vitro biocompatibility testing of Deionized water and PAA-hydrogel-conditioned medium was used as a control.

1D touch strip: A PC-OH touch strip (10.0 × 3.0 × 0.2 cm) was made, and copper electrodes (1.0 × 1.0 cm) and a current meter (multimeter, model 34461A, Agilent) were connected to the two ends of the touch strip. A function generator (model 33612A, Agilent) was connected to the two parallel current meters, and an AC current of the same phase was applied to both sides of the PC-OH strip. The strip was touched with a finger to show the relationship between touch position and current, which was recorded by the current meters at each touch point. The strips were then stretched to twice their original length and touched with a finger in stretch mode. In these cases, the measured currents were recorded at temperatures of -20, 25, and 60°C with an AC voltage of -3.0 ~ 3.0 V at a frequency of 17 kHz generated by the function generator. Unless otherwise stated, the samples in this study were stored at the test temperature for at least 12 hours. To study the sensing ability of the touch strip in a wet environment, the touch strip was sprayed with water and then allowed to air dry for a

different time, resulting in different levels of wetness (wet, dampish, and recovery). To study the electrical self-healing ability of the touch strip, it was also cut with a sharp ceramic knife, and the freshly cut parts were rejoined.

The sensing mechanism of 1D touch strip: A 1D touch strip was used to study its sensing mechanism because a 1D model simplifies the description of the current flowing through the PC-OH touch sensing system. The model consists of two resistors and three capacitors for the cut and connected strip. When a human finger touches the strip, the current can flow from the copper electrodes to the ground through the strip. The touch position can calculate the resistance values of the two resistors:

$$R_1 = \alpha R + R_l \quad (1)$$

$$R_2 = (1 - \alpha R) + R_r \quad (2)$$

where R is the original uncut strip total resistance and α is the normalized position, and R_l and R_r are the additional resistances introduced by the not fully healed interface between the touch point and current meters A1 and A2, respectively. Each resistor is connected with a capacitor C_{EDL} in series. Therefore, the impedance Z of the two parts can be determined as follows:

$$Z_1 = R_1 - j\frac{1}{2\pi f C_{EDL}},\ Z_2 = R_2 - j\frac{1}{2\pi f C_{EDL}} \quad (3)$$

Since the capacitance per unit area of the double layer C_{EDL} is about 10^{-1} F/m^2; the area of the double layer is about 6×10^{-5}/m^2, and the current frequency is around 17 kHz, the reactance of the double layer is $-j\frac{1}{2\pi f C_{EDL}} \approx -1.6j$. As this reactance is much smaller than the resistance of the PC-OH touch strip (R ~ 3300 Ω, T = 25 °C), the impedance is $Z = 3300\Omega - 1.6j \approx 3300\angle -0.028$ and can be approximated by the resistance value ($Z \approx R$), so that the ratio of the two resistances can be used to calculate the touch current. The voltages on the two resistor parts are :

$$U_1 = I_1 \cdot Z_1 \approx I_1 \cdot R_1 \approx \alpha I_1 \cdot R + I_1 \cdot R_l = (\alpha + k_1) I_1 \cdot R \quad (4)$$

$$U_2 = I_2 \cdot Z_2 \approx I_2 \cdot R_2 \approx (1 - \alpha) I_2 \cdot R + I_2 \cdot R_r = (1 - \alpha + k_2) I_2 \cdot R \quad (5)$$

where K_1 and K_2 are the ratios of the healing interface-induced additional resistance, which is related to the total resistance of the uncut strip.

The two resistance parts are in parallel connection, and the voltages U_1 and U_2 on the

two resistances are the same with $K_1 = K_2$, thereby:

$$(\alpha + k_1)I_1 \cdot R = (1 - \alpha + k_2)I_2 \cdot R \quad (6)$$

$$\alpha = \frac{I_2}{I_t} + \frac{K_2 I_2 - K_1 I_1}{I_t} \quad (7)$$

where I_t is the circuit's current, and I_t can be expressed as $I_t = I_1 + I_2$.

The original and electrically completely recovered strip with:

$$K_1 = K_2 = 0 \quad (8)$$

$$\alpha = \frac{I_2}{I_t} \quad (9)$$

2D touch panel: Each corner of the PC-OH touch panel (8.0 × 8.0 × 0.2 cm) is connected to a copper electrode and then connected to the controller board by a copper wire. For optimal accuracy, the MT 7 software control panel (version 7.14.9) was used as a calibration tool provided by the controller board manufacturer is used. Since the output figures were not suitable for display when the 2D PC-OH touch panel was operated for the first time, a three-point calibration was performed to improve touch accuracy.

Wearable touch panel: VHB™ 4910 tape was used as an insulator to create a wearable touch panel. The PC-OH touchpad adhered to a VHB film, and copper electrodes were connected to the four corners of the touch panel. The assembled wearable touch panel can then be attached to the human body without losing function. When attached to the human arm, the wearable touch panel is entirely transparent, allowing the arm underneath the touch panel to be visible and also allowing successful operation. The function generator provides an AC voltage of -0.3 to 0.3V at a frequency of 17kHz.

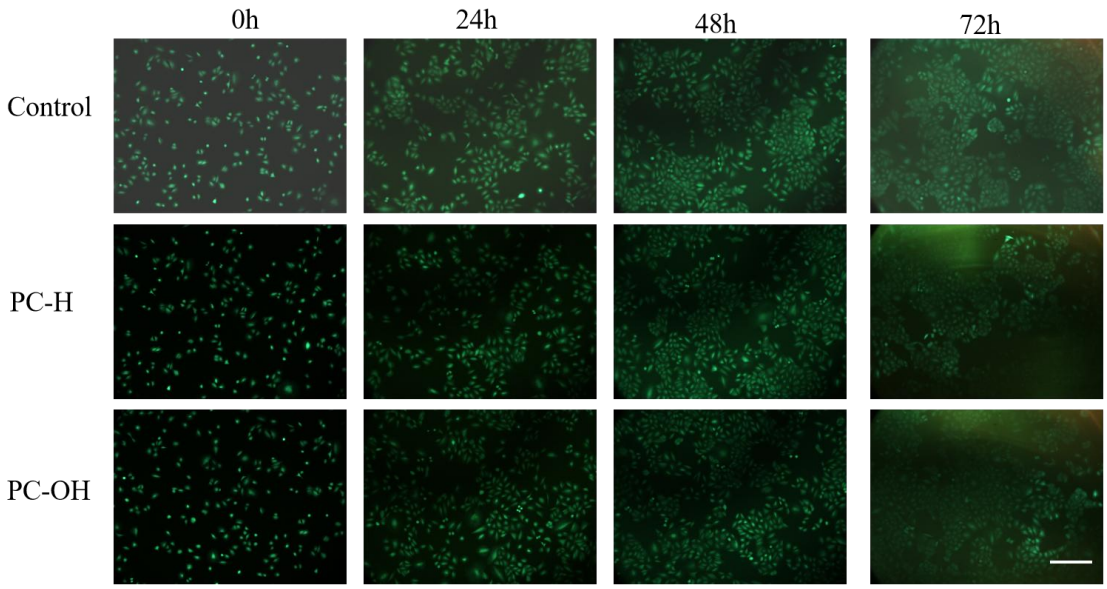

Fig. S1. In vitro biocompatibility studies of and PC-H and PC-OH in proliferation assay of A549 cells after culturing for different durations (0h, 24h, 48h, and 72h). Control: Deionized dwater (Milli-Q, 18.2 MΩ cm^{-1}). Scale bar: 250 μm.

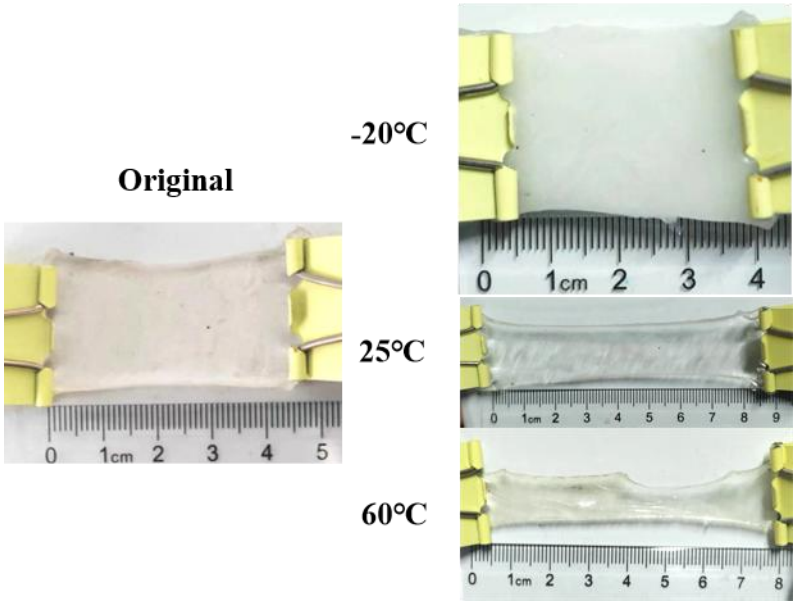

Fig. S2. Digital photos of original and tensile performance of PC-H at -20, 25, and 60 ℃ for 24h.

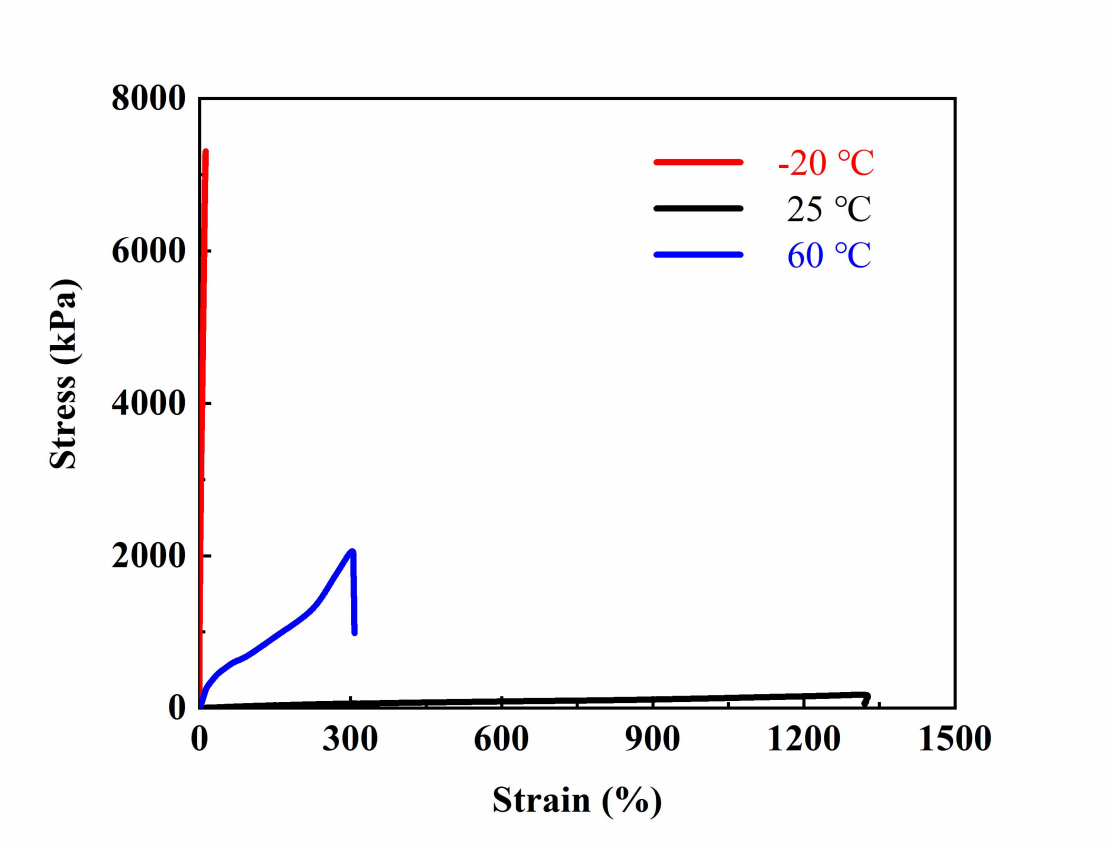

Fig. S3. Stress-strain curves of PC-H at different temperatures (-20, 25, and 60 ℃).

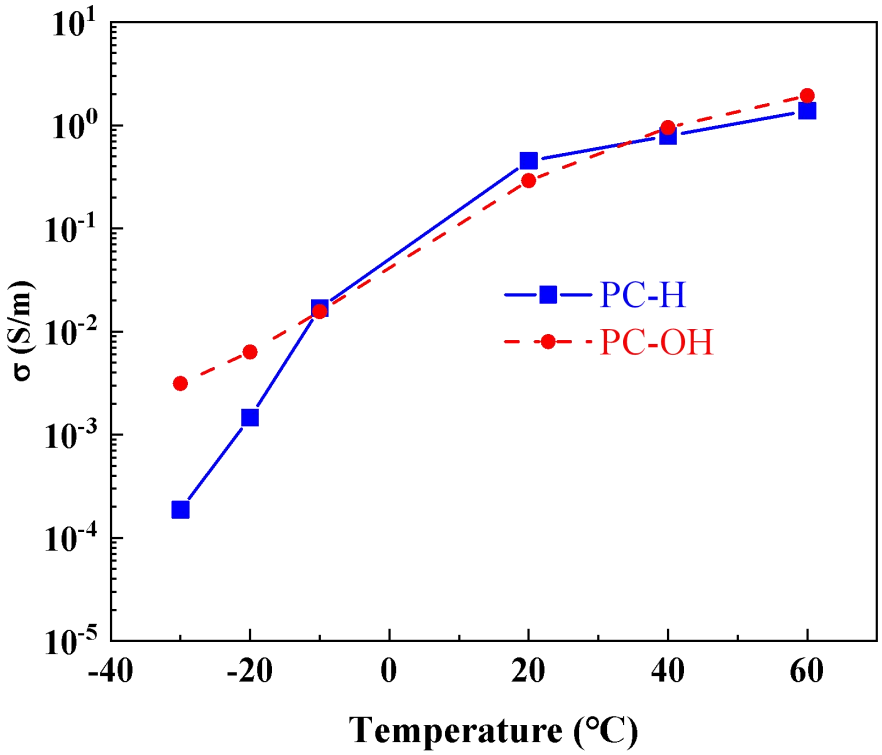

Fig. S4. The ionic conductivity of PC-H and PC-OH as a function of the temperature in the range of –30 to 60 ◦C.

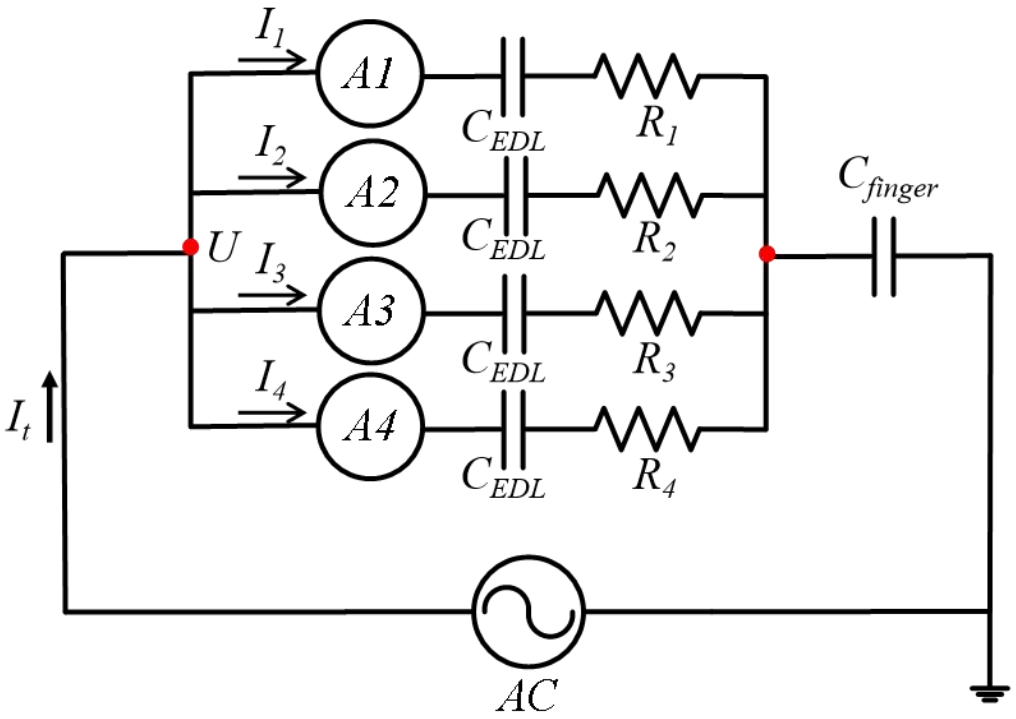

Fig. S5. Equivalent circuit diagram of the PC-OH touch panel when a finger touches it.

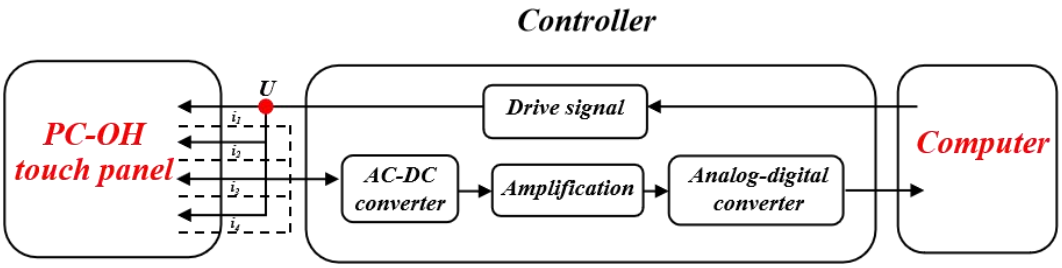

Fig. S6. Schematic diagram of the integrated PC-OH touch system.

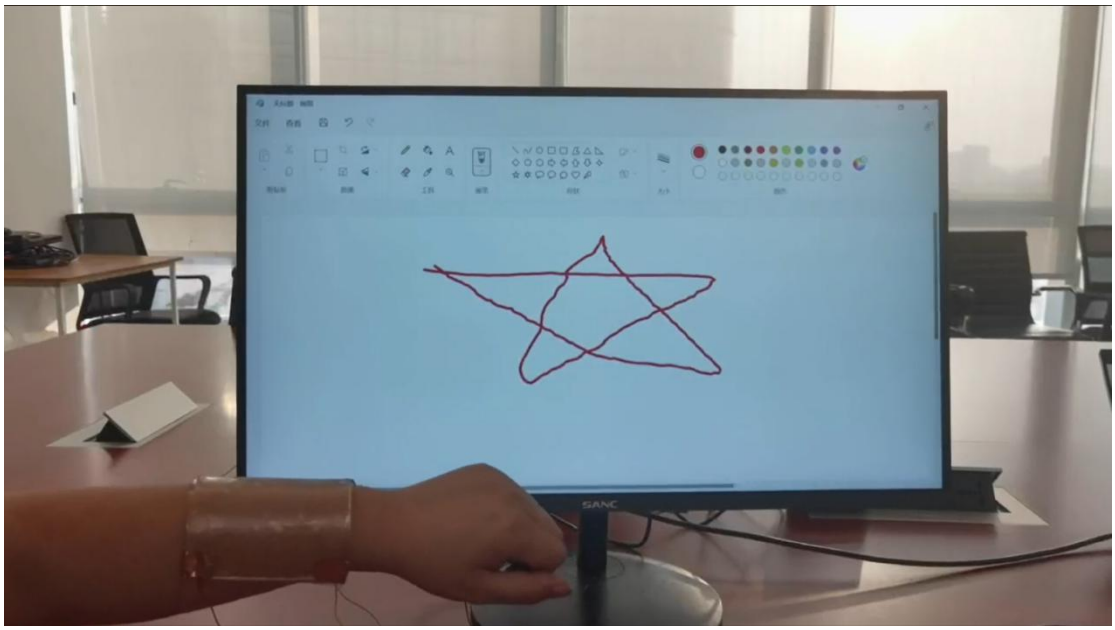

Fig. S7. The ability of the touch panel for drawing figures.

Table. S1: Input position (α, β), measured I_1, I_2, I_3, and I_4, calculated a and b, and calculated output position (α, β) of the five touch-points at -20, 25 and 60 ℃ in Figure 5a.

Temperature (℃)	Touch point	Input position		I_1	I_2	I_3	I_4	Output position	
		α	β					α	β
								(I2+I3)/(I1+I2+I3+I4)	(I1+I2)/(I1+I2+I3+I4)
-20	TP#1	0.25	0.75	3.205	0.888	0.583	0.862	0.266	0.739
	TP#2	0.75	0.75	0.861	3.191	0.833	0.646	0.728	0.733
	TP#3	0.75	0.25	0.585	0.806	3.268	0.760	0.752	0.257
	TP#4	0.25	0.25	0.838	0.613	0.855	3.206	0.266	0.263
25	TP#1	0.25	0.75	5.207	1.283	0.757	1.258	0.240	0.763
	TP#2	0.75	0.75	1.333	5.159	1.265	0.792	0.751	0.759
	TP#3	0.75	0.25	0.779	1.398	5.320	1.278	0.766	0.248
	TP#4	0.25	0.25	1.345	0.785	1.485	5.115	0.260	0.244
60	TP#1	0.25	0.75	5.870	1.502	0.799	1.402	0.240	0.770
	TP#2	0.75	0.75	1.462	5.821	1.422	0.756	0.766	0.770
	TP#3	0.75	0.25	0.819	1.537	5.863	1.538	0.758	0.241
	TP#4	0.25	0.25	1.496	0.804	1.495	5.872	0.238	0.238

Movies:

Movie 1. Self-healing process of the PC-OH sample under the optical microscope.

Movie 2. A touch panel is used to draw a smiling face.

Movie 3. A touch panel is used to draw two concentric squares.

Movie 4. The touch panel can be used to draw the same concentric squares after pouring water on the touch panel.

Movie 5. The touch panel is cut into two parts and heals after 24 hours, and then is used to draw the same concentric squares.

Movie 6. The touch panel is cut into four parts and heals after 24 hours, and then is used to draw the same concentric squares.

Movie 7. A touch panel is adhered to the arm and then is used to write the word "THU."

Movie 8. The same wearable touch panel is used to draw pentagrams.

Movie 9. The same wearable touch panel is used to play the computer game "Angry Birds."